TECHNICAL UNIVERSITY OF LIBEREC
Faculty of Mechatronics, Informatics
and Interdisciplinary Studies

Development of methods for surface topography measurement with sub-nanometer accuracy

Master thesis

Study programme: B3901 – Applied Sciences in Engineering
Study branch: 3901R055 – Applied Sciences in Engineering

Author: **Bc. Karolína Sedláčková**
Supervisor: Ing. Pavel Psota, Ph.D.
Consultant: Christian Schober, Ms. c.

Liberec 2021

TECHNICKÁ UNIVERZITA V LIBERCI
Fakulta mechatroniky, informatiky
a mezioborových studií

Vývoj metod pro měření topografie povrchu se subnanometrovou přesností

Diplomová práce

Studijní program: B3901 – Aplikované vědy v inženýrství
Studijní obor: 3901R055 – Aplikované vědy v inženýrství

Autor práce: **Bc. Karolína Sedláčková**
Vedoucí práce: Ing. Pavel Psota, Ph.D.
Konzultant: Christian Schober, Ms. c.

Liberec 2021

TECHNICKÁ UNIVERZITA V LIBERCI
Fakulta mechatroniky, informatiky
a mezioborových studií

Zadání diplomové práce

Development of methods for surface topography measurement with sub-nanometer accuracy

Jméno a příjmení: **Bc. Karolína Sedláčková**
Osobní číslo: M19000182
Studijní program: N3901 Aplikované vědy v inženýrství
Studijní obor: Aplikované vědy v inženýrství
Zadávající katedra: Ústav nových technologií a aplikované informatiky
Akademický rok: **2020/2021**

Zásady pro vypracování:

1. Seznámení se s principy bezkontaktních metod pro měření topografie povrchu.
2. Vytvoření numerického nástroje pro analýzu koherenční skenovací interferometrie.
3. Testování, analýza a optimalizace vyvíjeného profilometru NPMM-200.
4. Celkové zhodnocení výsledků.

Rozsah grafických prací:	dle potřeby dokumentace
Rozsah pracovní zprávy:	40 – 50 stran
Forma zpracování práce:	tištěná/elektronická
Jazyk práce:	Angličtina

Seznam odborné literatury:

[1] MALACARA, D. Optical shop testing. 3rd ed. Hoboken, N.J.: Wiley-Interscience, c2007. ISBN 0471484040.
[2] SALLEH, B. E. A. , TEICH, M.C.: Základy fotoniky I,II , MATFYZPRESS, Praha, 1994-95.

Vedoucí práce:	Ing. Pavel Psota, Ph.D. Ústav nových technologií a aplikované informatiky
Datum zadání práce:	19. října 2020
Předpokládaný termín odevzdání:	17. května 2021

L.S.

prof. Ing. Zdeněk Plíva, Ph.D.
děkan

Ing. Josef Novák, Ph.D.
vedoucí ústavu

V Liberci dne 3. října 2019

Prohlášení

Prohlašuji, že svou diplomovou práci jsem vypracovala samostatně jako původní dílo s použitím uvedené literatury a na základě konzultací s vedoucím mé diplomové práce a konzultantem.

Jsem si vědoma toho, že na mou diplomovou práci se plně vztahuje zákon č. 121/2000 Sb., o právu autorském, zejména § 60 – školní dílo.

Beru na vědomí, že Technická univerzita v Liberci nezasahuje do mých autorských práv užitím mé diplomové práce pro vnitřní potřebu Technické univerzity v Liberci.

Užiji-li diplomovou práci nebo poskytnu-li licenci k jejímu využití, jsem si vědoma povinnosti informovat o této skutečnosti Technickou univerzitu v Liberci; v tomto případě má Technická univerzita v Liberci právo ode mne požadovat úhradu nákladů, které vynaložila na vytvoření díla, až do jejich skutečné výše.

Současně čestně prohlašuji, že text elektronické podoby práce vložený do IS/STAG se shoduje s textem tištěné podoby práce.

Beru na vědomí, že má diplomová práce bude zveřejněna Technickou univerzitou v Liberci v souladu s § 47b zákona č. 111/1998 Sb., o vysokých školách a o změně a doplnění dalších zákonů (zákon o vysokých školách), ve znění pozdějších předpisů.

Jsem si vědoma následků, které podle zákona o vysokých školách mohou vyplývat z porušení tohoto prohlášení.

17. května 2021 Bc. Karolína Sedláčková

Abstrakt

Cílem práce bylo vyvinout simulační software, který zkoumá vliv vibrací na signál získaný z white-light interferometrie a aplikovat získané dovednosti ve vývoji vývoji nanopozičního měřícího zařízení pracujícího na výše zmíněném principu. Teoretická část je věnována popisu vlastností světla a popisu optických metod pro zkoumání topografie povrchu. Díky popsaným principům bylo možné zlepšit měřící zařízení a zvýšit jeho konkurenceschopnost.

Klíčová slova: topografie, měření topografie povrchu, white-light interferometrie, vibrace

Abstract

The aim of the thesis was to create a simulation tool inspecting the influence of vibration to evaluate the signal obtained from white-light interferometry. The theoretical part is dedicated to introducing the properties of different illumination sources and describing optical methods for examining surface topography. The knowledge gained while working with the simulation tool was applied to the development of a nanopositioning measuring machine based on the white-light interferometry. The applied approaches led to improving the machine and increasing its competitiveness.

Keywords: topography, surface topography, white-light interferometry, vibrations

Acknowledgements

I would like to express my sincere gratitude to everyone from ITO for accepting me to become a part of the team, namely Christan Schober Ms.C. and Dipl.-Phys. Christof Pruss for professional help and endless amount of consultation.

I wish to show my gratitude to Ing. Pavel Psota, Ph. D. for making the internship possible and for supervising my thesis again.

I would also like thank to my boyfriend who gives me uncountable amount of rides from home to Stuttgart and back. Thank to my parents for making my internship financially possible. I would also like to thank miss Michaela Indrisekova for finding a time while relaxing in a spa to be the proofreader.

Contents

List of Figures

List of abbreviations

WLI	White light interferography
nm	nanometr
um	micrometr
STEM	scanning transmission electron microscopy
NPMM-200	Nanopositioning measuring machine 200
TEM	transmission electron microscope
SEM	scanning electron microscope
OPD	optical path difference
COG	center of gravity
c	speed of light in vacuum
t	time
RMS	root mean square
LED	light emitting diode
E	intensity of electric field
λ	wavelength
λ_p	peak wavelength
μ	frequency
r	spatial vector
I	intensity of the light
d	distance
NA	numerical aperture
l_c	frequency
I_B	background intensity
γ	sampling contrast
φ_0	phase difference
ITO	Institut für Technische Optik
FFT	Fast Fourier transformation

Introduction

Topography gives us information about characteristics of spatial distribution and pattern of the element. It is used to detect irregularities on the element's surface. In the optical elements these irregularities can lead to erroneous imagining.

History of measuring topography of surfaces dates back to 1930s. The original analyzers were only mechanical, made up of a small needle moving across the surface. Later on, analogue particles were added and the result was formed by averaging signal from the moving needle. Unfortunately, the resolution from theses approaches was not sufficient enough for increasing claim to precise measurement. Later on, new measuring instruments were introduced, for example interference microscope and scanning transmission electron microscope (STEM). Better axial resolution came with digital computing. One of the biggest inventions in topography measurement came with an invention of a scanning tunnelling microscope followed by an atomic force microscope. They both provide nanometer to sub-nanometer resolution. This thesis is focused on inspecting surface topography with optical interferometers. These measuring approaches are fast, non-invasive and with an axial resolution over 1 nm.

This thesis has two outcomes; the first one being a simulation tool for coherence scanning (also called as white-light) interferometry, where we can see how different shapes of surface, size, wavelength and other properties are influencing the final envelope of signal. The white-light inteferometer measures surface topography with evaluating the signal wavelet. The result of the simulation tells us if vibrations can influence the measurement and if we really need a nanopositioning measuring device. It describes measuring with a white-light interferometer. The roughness of the surface and vibrations complicates processing of the signal. The influence of the vibrations is explored in the numeric tool. This tool takes the signal, adds vibrations and reduces the influence of vibrations to the signal.

The second part is development and verification of measuring device NPMM-200. The device was invented at Technical University of Illmeau. One machine was

bought by Institut für Technische Optik, Universität Stuttgart, where the tests and experiments are going to made this machine a decent competitor to commercial machines. This device is able to measure the shape and topography of various samples in sub-nanometer resolution. In the thesis, different measurement approaches are described. The approaches were tested to find the best way to measure a certain shape. To obtain the sub-nanometer resolution, it is necessary to have the device in stable conditions - even the changes in the atmospheric pressure can influence the results. We also compare NPMM-200 with commercial measuring device Zygo, based on white-light interferometry. For verification, we measured several samples with different shape and material. We controlled the machine with programs in ITOM and the data were evaluated in MATLAB. The thesis is focused of measuring surface topography with Nanopositioning measuring machine NPMM 200.

1 Illumination

1.1 Sources of the light

Light comes to us from different sources. The source that has the most important influence to our lives is the Sun. The light coming from the Sun has a broad spectrum of the radiation, ranging from 100 nm to 1,000,000 nm. Radiation with the wavelength from 100 to 380 nm is called an ultraviolet light. Ultraviolet radiation cannot be seen by human eye. Most of the ultraviolet spectrum is absorbed by the ozone layer of the Earth, but some of it can penetrate the layer and thus be harmful to people. The light visible to the human eye has a wavelength from 380 to 700 nm. The radiation with wavelength greater than 700 nm is called an infrared. Infrared radiation is also thermal radiation. [1], [2]

Until nineteenth century the only source of light came from natural sources (fire, sun) but in 19th century, there were first attempts with an artificially generated light - light bulbs. [3]

1.1.1 Light - emitting diode

In the 1960s, another source of light was invented - a light-emitting diode (LED). LED is based on the principle of glowing semiconductors in electric field. LED is producing white light by using blue LED and a phosphor layer. The color of phosphor influences the final spectrum. The spectrum has a Gaussian shape with peak wavelength λ_P [4].

The diode is made of p and n type semiconductors. The p type semiconductor provides electron a "hole" (it has three electrons in the valence band), n type semiconductor provides free electrons (has five electrons in the valence band). LED must be in forward bias setup to emit light. The cathode of the diode is connected to the negative side of a voltage source, anode is connected to the positive side of a voltage source. When the current goes through the circuit, the free electrons from n semiconductor have a tendency to fill the holes in p semiconductor. During the

crossing between the types, the free electrons release energy and fill empty holes in the valence band. The energy discharged during the process of recombination turns to the light. The color of the light changes with the used material. The white light can be obtained in multiple ways - combining the blue LED and the yellow phosphor or combining three different colors of LED red, blue and green. [5], [6], [7], [8]

1.1.2 Laser

There are also sources of radiation producing coherent light. Coherent light is used in many measurement areas. It is important for standard interferometry. Most types of interferometers work with a coherent source of light, such as lasers. [9], [10]

Laser is an acronym for "Light Amplification by Stimulated Emission of Radiation". The light from lasers is created by a stimulated emission, as the name suggests. There are multiple energy levels in an atom. An electron of the atom is in a ground level with energy E_1. When energy from light or heat is absorbed by an electron, the electron is excited to higher energy level E_2. The electron is not able to stay in the higher energy level, when there is energy influencing the electron (energy from light with frequency ν), the electron is going back to the base energy level. During the process, light can be radiated. Radiated light has the same frequency ν. [10], [11]

Atoms have exactly two energy levels - ground level and higher energy level (excited level). The light is amplified only by atoms in excited level. The atoms in ground level absorb energy in form of light. The absorption brings electrons to the excited level. This process leads to amplification but occurs only when more than 50% of electrons are in a higher energy level. This process is called population inversion. [9], [11]

The standard laser is made up of an active medium (the part where the electron pumping is made). For light generating, an optical resonator is used. One of the mirrors is partially transparent. The active medium can be in solid, liquid, gas or plasma state. [9][12] [13]

The light coming from a laser is coherent. Usually, it is demanded to have a light with a high degree of spatial and time coherence. The wavelength of the light differs with the used active medium. For example: one of the lasers that is used the most in the metrology is helium - neon laser. This laser has operational wavelength 632.8 nm, but it can also be different (e. g. 543.5 nm, 593.9 nm, 611.8 nm) [14]. [10]

1.2 Coherence

Coherence can be described as the statistical representation of quasi - monochromatic wave. Let E($\mathbf{r}$, t) be the wave defined by the position of vector $\mathbf{r}$ (x,y,z) and t is time. The description of wave fluctuating in field is specified by a cross-correlating function. The cross-correlation function depends on the difference between the two time arguments. This difference is called $\tau = t_2 - t_1$. The cross- correlating function is also known as the mutual coherence function and is described below.

$$\Gamma(\mathbf{r}_1, \mathbf{r}_2, \tau) = \langle E^*(\mathbf{r}_1, t) E(\mathbf{r}_2, t + \tau) \rangle \tag{1.1}$$

The equation represents the wave in space and time. The "*" symbol stands for a complex conjugate of a complex number. [15].

The white light is a spectrum of waves with different wavelengths. The coherence function of the white light is defined by function [16]

$$\Gamma(\mathbf{r}_1, \mathbf{r}_2, \tau) = \sum_i \langle E_i^*(\mathbf{r}_1, t) E_i(\mathbf{r}_2, t + \tau) \rangle. \tag{1.2}$$

There are two types of coherence - spatial and temporal coherence. Spatial coherence describes how the phase of electromagnetic wave correlates at the different points of space.

Temporal coherence describes how the electromagnetic waves correlate at the same point in different time. The degree of temporal coherence is qualified by the coherence time. For light field with constant statistical properties is the coherence time defined as

$$g(\tau) = \frac{\langle E^*(t) E(t + \tau) \rangle}{\langle E^*(t) E(t) \rangle}. \tag{1.3}$$

E is an electromagnetic wave andτ is a time delay. The equation 1.3 can be rewritten to an arbitrary shape as

$$\tau_c = \int_{-\infty}^{\infty} |g(\tau)|^2 \, d\tau \tag{1.4}$$

In interferometers, the coherence beam is crucial for seeing the interference fringes with a naked eye. **More than coherence time is the coherence length usually used.** [19]. A good visibility of the fringes is given by a long coherence length [17]. The coherence length is defined by spectral linewidth ($\Delta\lambda$) and wavelength.

$$Lc = 0.44 \frac{\lambda^2}{\Delta\lambda} [air] \tag{1.5}$$

Sources with a short coherence are LED or broadband lasers, sources with long coherence length are lasers.

1.3 Diffraction

The first description of the light propagation was described by Huygens, thus, this descriptions is known as the Huygens principle. The Huygens principle says that every point of the wavefront can be a source of secondary wavelets. In 19th century, the Huygens principle was amended by Fresnel. Later, the description was more specified - every point of the wavefront can be source of spherical secondary wavelets, with the same frequency as the primary wave. The resulting amplitude of the optical field is a superposition of all the wavelets in it.When a light wave meets an obstacle, it may reflect or bend itself. The bending is called diffraction. Diffraction is a special type of light scattering. [20]. Diffraction can be described by approximations.

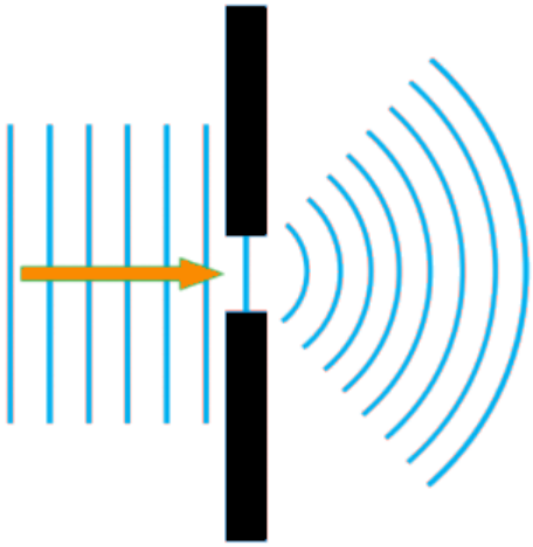

Figure 1.1: Diffraction

1.3.1 Fraunhofer diffraction

This phenomenon is also called the "far field diffraction". It is described on parallel beam. The shape of the bending phenomenon is determined from the shape and dimensions of the obstacle. Let S be the point source of the light, P is a viewing point. If both points are far enough from the obstacle with a small aperture d, the light waves are planar. In Fraunhofer diffraction there is the linear dependence on

aperture variable. Diffraction differs by an obstacle, there are different conditions if the diffraction is on the single slit, rectangular aperture or the circular aperture. The next section focuses on the Fraunhofer diffraction on the circular aperture.

Diffraction on the circular aperture Let the circular aperture be divided into strips with the width dy and length $l = 2\sqrt{r^2 - y^2}$, where r is a radius of the aperture. Then the amplitude of incident light will be

$$E = \frac{2E_A}{\pi r^2} e^{i(\omega t - kR)} \iint_{Aperture} e^{ikysin\nu} \sqrt{r^2 - y^2} dy, \tag{1.6}$$

where E_A is amplitude of electromagnetic field per unit of area of the aperture, k is a wave number, R is a distance between a P point and center of the aperture and ν is an angle between the planes.

Firstly it is necessary to substitute the r, y, k and ν, with two new variables, u and ρ to obtain intensity. $u = y/r, rdu = dy$ and $\rho = rksin\nu$. Then the integral in eq. 1.6 can be rewritten as

$$\int_{-1}^{1} e^{i\rho u} \sqrt{1 - u^2} du. \tag{1.7}$$

The intensity of the diffracted light can be expressed with the first kind of Bessel function of first order - $\frac{\pi J_1(\rho)}{\rho}$. Therefore the intensity is described by

$$I = I_0 \Big[\frac{J_1(\rho)}{\rho} \Big]^2 \tag{1.8}$$

From the course of the function, it can be seen that the most of the intensity is focused to the circle situated in the center. This circle is called the Airy disc. When the Bessel function equals zero. This minimum is set when $sin\nu = 1.22\frac{\lambda}{2r}$. [9] [20], [21] [22]

1.3.2 Resolution

The principles from Fraunhofer diffraction lead us to the resolution of optical setups. The resolution is given by Rayleigh criterion.

It says that *"two images are just resolvable when the center of the diffraction pattern of one is directly over the first minimum of the diffraction pattern of the other"*. [23]

In case of the circular aperture, it is described by the angular limit $sin\nu = 1.22\frac{\lambda}{2r}$.

Hence, all the attempts are limited by the wavelength. The light source with a short wavelength can be used. There are also limitations in recognizing far objects such as stars. The resolution my be improved by increasing the size of the lens or mirror in the telescope. In a microscope, the resolution is given by a numeric aperture (NA). Numeric aperture is described by equation $NA = nsin(\theta)$, where n is a refraction index and θ is angle of light entering to the microscope objective. [9] [20], [23]

1.4 Interference

The light can be seen as an electromagnetic wave. The interference is a superposition of more than one wave. Let there be two waves $E_1(\boldsymbol{r}, t)$ and $E_2(\boldsymbol{r}, t)$. As result light field described in equation below is obtained

$$E(\boldsymbol{r}, t) = E_1(\boldsymbol{r}, t) + E_2(\boldsymbol{r}, t), \tag{1.9}$$

Where $\boldsymbol{r}$ is a position vector and t is time. But eyes and detectors are only able to detect intensity of the electromagnetic wave $I \approx E^2$. When two waves met, the final intensity is not equal to sum of these two wave. Each wave can be described by function

$$E(\boldsymbol{r}, t) = \frac{1}{2}[E_{12}(\boldsymbol{r})e^{-i\omega t} + E_{12}A^*(\boldsymbol{r})e^{i\omega t}], \tag{1.10}$$

the result can be counted as the electromagnetic field with complex amplitude. The intensity is counted as

$$I(\boldsymbol{r}) = E(\boldsymbol{r})E^*(\boldsymbol{r}). \tag{1.11}$$

Then the equation can be rewritten as the interference of two waves as

$$I(\boldsymbol{r}) = I_1 + I_2 + E_1E_2^* + E_1^*E_2 = I_1 + I_2 + \mathfrak{Re}\{E_1 + E_2^*\}, \tag{1.12}$$

therefore

$$I = I_1 + I_2 + 2\sqrt{I_1I_2}cos\alpha, \tag{1.13}$$

where α is a phase difference between the waves in given space. [9],[24],[22]

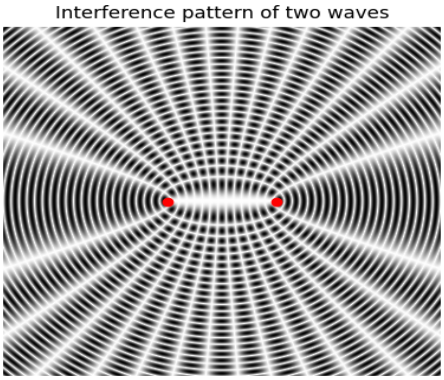

Figure 1.2: Interference pattern of two waves

2 Measuring surface topography

During the surface topography measuring, roughness on the small scales, a profile and an area of the sample on the larger scales may be observed. There are several approaches how to get information about the sample. The ISO standard of surface roughness is ISO 1320. This standard is describing requirements for technical drawings as well as roughness symbology [25]. Methods based on contact with the sample such as roughness meter can be used [26]. This type of measuring devices has the scanning probe, that is moving on the sample surface. For measuring with high precision, it is suitable to use measuring methods based on optics. [26]

2.1 Interferometry

The basics of interference is described in 1.4. The interferometers can analyse how the light properties are changing at given surface. The interferometeres with more than one path of the light beams are suitable for measuring areal surface topography. The intensity of the interfering light is changing with the differences of the optical paths lengths. [27]

2.1.1 Michaelson interferometer

A standard Michaelson interferometer composes of a laser, two mirrors, a beam splitter, and a detector. The first concept of this type of interferometer was introduced in 1881 [28]. This deviced is based on splitting a beam by a beam splitter. The splitted beams go to mirrors, are reflected from the mirrors, are recombined again in the beam splitter and interfere with each other. The interference is possible because the beams are coherent. The recombined beams go to the sensor. [29]

With a few upgrades, the Michaleson interferometer can be transformed into a device for measuring areal surface topography. These upgrades are made by adding lenses around the beam splitter in order to extend or collimate the beam and the camera that are sending signal to evaluation. [27]

With a few modifications, the Twyman-Green interferometer can be made. The Twyman-Green setup was made for testing of microscope objectives and later on updated for measuring camera lenses. In contrast to the Michelson setup, there is a compensator added in front of one mirror in this setup. With changes in optical path difference (OPD), it is possible to measure thickness. Testing prisms is possible due to a change of direction of perfectly straight lines. [30]

2.1.2 Mach-Zehnder interferometer

Mach-Zender interferometer is made of the source of the light, two beamsplitters, two mirrors with a total reflection, and a detector. The first beamsplitter divides the beam from the source into two paths. Those beams are recombined after transiting through the second beamsplitter. If there is an object given to one branch of the interferometer, the difference between the paths occurs.[22] [31]

This type of interferometer is also used in digital holographic microscopy (DHM). In the Mach-Zehnder, it is divided with beamsplitter into two branches - the objective branch and the reference branch. The light going into the reference branch leads up directly to the second beamsplitter. The light in reference branch is going through the sample and microscope objective. The light recombines in the second beamsplitter. The beam from the objective branch has a shifted phase besides the reference beam. With DHM, it is possible to measure surface topography as well as the shape of the given object.[27] [32]

2.1.3 Newton interferometer, Fizeau interferometer and Mirau interferometer

Newton interferometer The Newton interferometer is built of the source of light, beamsplitter and two lenses, which are divided from each other with a small air gap. The light recombines after transmitting the convex lens. One of this lenses is convex and the other is planar. The light from the source is divided into multiple beams. Beams are reflected by the lenses. One of the beams is reflected from surfaces of the lenses internally, others are reflected externally. Due to this, there is an optical path difference between the reflected beams and a phase change by π rad. This phase difference causes dark fringes in the interferometer.[33]

The Newton interferometer can be used for measurement of spherical and aspherical surfaces and flatness of opaque surfaces.

Fizeau interferometer Fizeau interferometer is based on the principle of the Newton interferometer, but the Fizeau interferometer has a broader air gap and a spatial filter, just after the light source. The extension of the gap puts lower demands on the surface purity. However, there is a requirement on the strength of the light source and a necessity to collimate the beam with a high quality collimator. The light beams go to the collimating lens.The Collimated beams transmit to the tested surface and then are reflected flat. The reflected beam is going through the reference surface and the collimator to the beamsplitter. The beams recombine after the beamsplitter and the interference fringes are sent to the sensor.

This type of interferometer is used for measuring the quality of optical components and guiding component production. [33] [34]

Mirau interferometer The light from the source, which travels to the test surface, goes through the the microscope objective. Between the tested surface and the objective, there are two glass plates. One side of the plate is with an aluminized point, which is highly reflective, and is used as a reference point. The second plate has a modified surface used as a beamsplitter. The beams recombine at the beamsplitter and travel back to the objective. [33]

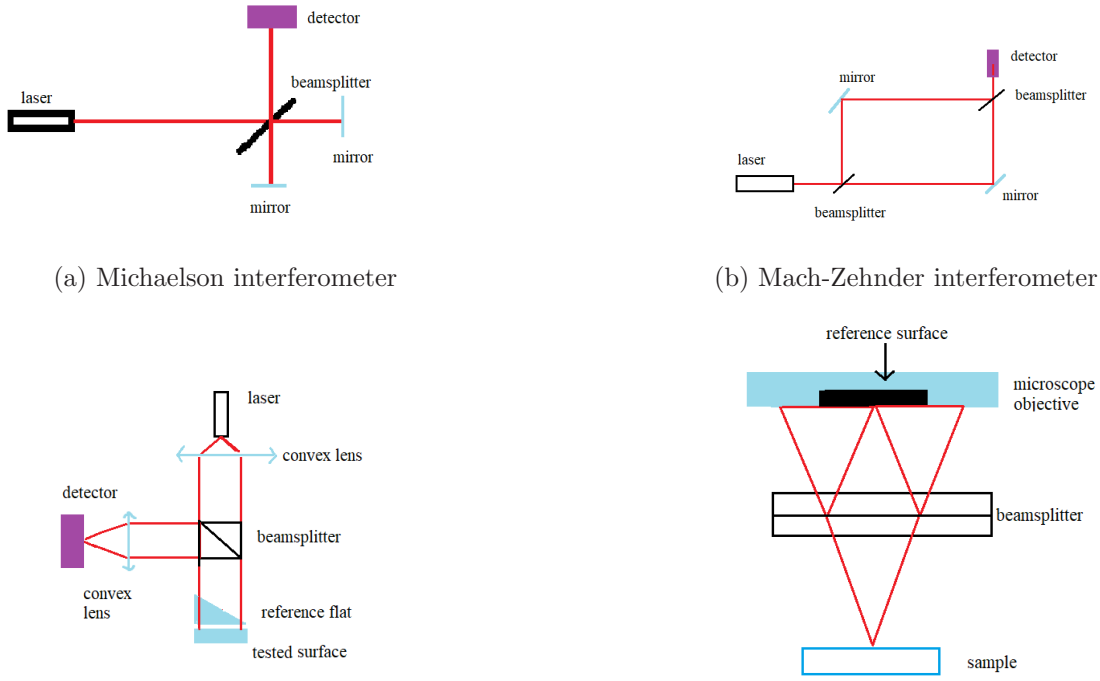

(a) Michaelson interferometer

(b) Mach-Zehnder interferometer

(c) Fizeau interferometer

(d) Mirau interferometer

Figure 2.1: Multiply with sinus - data with vibration

2.1.4 White light interferometry

White–light interferometry is an interferometry that uses different illumination sources compared to the usual interferometers. The problem lies within obtaining interference fringes because for using light with a short coherence length, it is necessary to match the paths of an interferometer. Using white-light source creates fringes for every wavelength and the intensity is got by summing these sets. In the WLI it is necessary to get zero optical path difference (OPD) to obtain white-light fringes. [35] [36]

The sample is inserted between two branches of the interferometer, the Michelson's setup can be used, as well as other setups, except for Fizeau. Then, the light reflected from the sample interferes with the light from the reference branch, then the intensity is recorded on camera sensor. The sample or the probe is moving. During the movement, the images are captured. From the each point of the captured figures taken during scanning along the z axis, the interferogram can be extracted, as shown in figure 2.2. The wight light arises by composition of light of all wavelengths[35],

[36] The signal can be described with the equation

$$I(z) = I_B + \gamma I_B exp\left[\left(-\frac{z - z_0}{l_c}\right)^2\right] \cos\left[\frac{4\pi}{\lambda_0}(z - z_0) + \varphi_0\right], \tag{2.1}$$

where I_B is background intensity, γ is sampling contrast, z is a scanning position along z axis, z_0 is the scanning position of z axis, where is the maximum of the envelope, l_c is coherent length of the source beam, λ_0 is the wavelength of source beam and φ_0 is phase difference between the object and reference beam.[37]

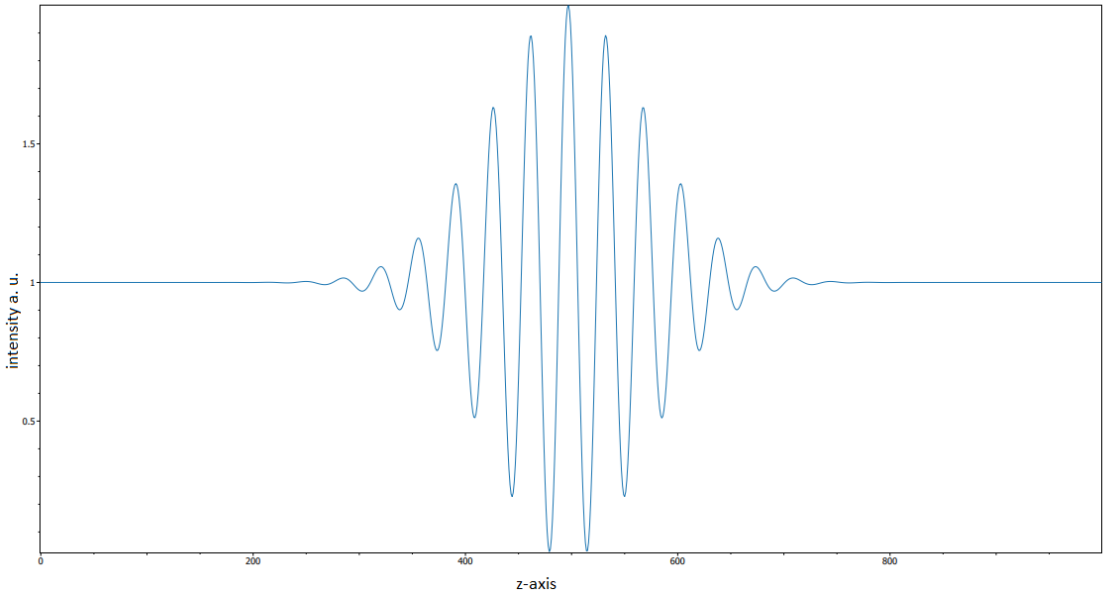

Figure 2.2: White-light interferogram

The zero OPD is in the position where the value of the signal envelope is the highest.

With WLI, we are able to measure optically rough surfaces. The maximal possible resolution is given by wavelength $\lambda/4$ of used light source. The roughness of the surface is causing development of speckles. The intensity of the speckle pattern gives us information about the root mean square of roughness. The roughness is causing decorrelation of the speckle pattern, therefore the interferogram is faulty. The deformed interferogram may arise even while measuring smooth patterns - if the step on scanning on the surface is smaller than the coherent length of the light source. During the evaluation of the sample, the maximum value of the interferogram and the center of gravity of the interferogram are compared. But if these two values are subtracted, the result is a number describing how much deformed the

interferometer is. [36] [37]

The center of gravity (COG) is an approach in signal processing. This value determines signal shifts as well as the envelope peak. The envelope peak is counted as a mass-weighted average location of the signal.

$$cog = \frac{\sum_{i=0}^{N-1} f(i)x(i)}{\sum_{i=0}^{N-1} x(i)}, \tag{2.2}$$

where *x(i)* is a weighted frequency value and *f(i)* is the center frequency of the signal.[38], [39]

2.2 Other measuring methods

The surface topography can be measured with methods, which are not based on interferometry.

Contact methods have a sharp stylus connected to a displacement transducer. The roughness is measured as a RMS of the profile from a reference line. Lateral resolution is given by the width of the stylus. [40] [41]

Ultra-high resolution profiling methods - into this methods scanning electron microscope (SEM) and transmission electron microscope (TEM) can be classified.

The resolution of the SEM is accomplished by the electron behavior similar to the wave behavior. With the potential difference up to 1000 V, the electron is accelerated and the de Broglie wavelength is 0.04 nm. Instead of a standard optic, magnetic lenses are used for focusing the electrons. The setup is build similarly to the optical microscope. The resolution is below 10 nm. [41] [42].

The electron beam is transmitted over a thin sample. During the transmission, the electron beam interacts with the testes sample. TEM has a better spatial resolution over SEM. Just like the SEM the TEM method uses electromagnetic optics. In this method, it is necessary to control the thickness of the tested sample, because the pores on the surface can negatively influence the measurement.[43] [44]

3 Simulation tool

The white-light signal is used for measuring with high precision and it is prone to vibrations. How the vibrations influence the signal determines the quality of the measurement. A simulation tool creates a plain with different shape, creates a white-light signal with vibrations and applies ITOM functions to get all the information about the signal.

ITOM is a software developed at ITO University of Stuttgart. The software is designed to operate measurement systems, data evaluation and automatizing laboratory devices. The software is fast, thanks to the C++ core but it is controlled with Python. The biggest advantage of using ITOM is its speed. It runs faster on older devices thanks to the C++ core.[45]

3.1 Evaluation of white - light interferometry

The explanation of the modules for white-light interferography are described in the paper [46]. The paper describes how the codes in simulation software are created.

The equation for signal generated in the paper is slightly different then the one that is used in the simulation software because the signal is generated for interferometer with two branches, reference branch z_R and objective branch z_O. The interference signal is given by the term

$$\begin{aligned} I_{LC}(\Delta\nu, \Delta k, k_0) &= I_R + I_O + 2(I_R I_O)^{1/2} \\ &*sinc\Big\{[2z_O - 2z_{R0} + y * sin(\alpha)]\frac{\Delta k}{2\pi}\Big\} \\ &*cos\{k_0[2z_0 - 2z_{R0} + y * sin(\alpha)] + \phi\}. \end{aligned} \tag{3.1}$$

The k_0 is a central wave number, I_R and I_O are the signals from reference and object wave, y is scanning position along spatial axis, ϕ is a phase. If the phase is 0, the position of center of gravity equals zero order interference fringe.

Before further evaluation of center o gravity and zero - order interference fringe,

a region of interest (ROI) is chosen. When the ROI is chosen, the moving average filter is applied to subtract DC offset from the raw data.

In the next step, the signal frequency to wave number k_0 is counted with the Fourier analysis, if the frequency is known, the modified interference signal is multiplied with "lock -in" function. The function has the same wave number k_0.

$$f_{LI} = exp(-ik_0 * \Delta z) \tag{3.2}$$

After tha,t the low pass filter is applied. The result of that is a smooth curve $I_{filtered}$. With the absolute square of $I_{filtered}$ the envelope $E(\Delta$ z) may be calculated.

$$E(\Delta z) = 2[\mathbb{R}(I^2_{filtered}) + \mathbb{I}(I^2_{filtered})]^{1/2} \tag{3.3}$$

From the envelope $E(\Delta$ z) the COG position along z axis is counted (z_{COG}). From this value, the OPD Δz is found out. This value correlates with the relative object position of object ($z_0, \Delta z = 2(z_0 - z_R)$). To get this value, it is necessary to find out the phase ϕ between the f_{LI} and the signal. This value is obtained by arctan of summing real and imaginary part of $I_{filtered}$.

$$\phi = arctan(\sum \mathbb{R}(I_{filtered}), \mathbb{I}(I_{filtered})) \tag{3.4}$$

Additionally, it is necessary to of find the phase of COG of F_{LI}. It is counted from as

$$\phi_{ZOG} = k_0 * z_{COG} \quad mod 2\pi. \tag{3.5}$$

From previously gained values, the distance Δz_R is counted. This value tells us the nearest position of z_{COG} and zero phase crossing position of the lock-in function $z_{\phi 0,L-I}$. The Δz_R value varies according to the value of phase

$$\Delta z_R = \begin{cases} \frac{-\phi_{COG}}{k_0} & \text{if } \phi_{COG} \leq \pi \\ \frac{2\pi - \phi_{COG}}{k_0} & \text{otherwise} \end{cases} \tag{3.6}$$

After finding ϕ_{ZOG} and Δz_R the value $z_{\phi 0,L-I}$ is obtained; $z_{\phi 0,L-I} = z_{COG} + \Delta z_R$. Now the zero phase crossing position of the signal to $z_{\phi 0,L-I}$ can be determined

$$z_{\phi 0} = z_{\phi 0,L-I} + \frac{\phi}{k_0} \tag{3.7}$$

The maximal value of phase error is half of a wavelength, because the domain of

*arctan*2 function is in interval $(-\pi, \pi]$. Thus, in the last step, it is necessary to check the distance between $z_{\phi 0}$ and z_{COG} differs for half for more then a half of the wavelength. If the distance is greater, the z_0 position must be corrected by $\pm\frac{\pi}{k_0}$.

$$z_O = \begin{cases} z_{\phi_0} + \frac{2\pi}{k_0} & \text{if } z_{COG} - z_{\phi 0} > \frac{\pi}{k_0} \\ z_{\phi_0} - \frac{2\pi}{k_0} & \text{if } z_{COG} - z_{\phi 0} < \frac{\pi}{k_0} \\ z_{\phi_0} & \text{if } -\frac{\pi}{k_0} \leq z_{COG} - z_{\phi 0} \leq \frac{\pi}{k_0} \end{cases} \tag{3.8}$$

In figure 3.1 is z_O and z_{COG} are shown for given region of interest.

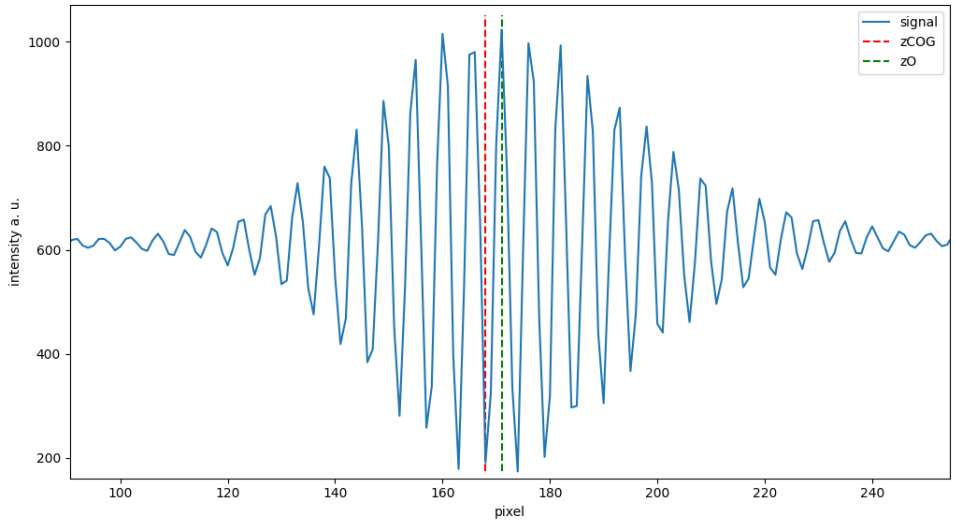

Figure 3.1: ROI of evaluated wavelength, z_{COG}, lock - in z_O

3.2 Software simulating influence of vibrations to white-light interferometry

In the paragraphs bellow are described function of simulation software.

3.2.1 Generate z0

Function generate z0 creates three dimensional array with chosen shape and size. The parameters of the function are:

Shape defines shape of simulated topography, shown in 3.2:

- line – simulated plane is shaped as line
- sine – simulated plane is shaped as sine wave
- sphere – simulated plane is shaped as sphere

Coefficient k, b define shape of sine wave. line – if k and b is defined, the topography is created by equation $topo = k * x + b * yc$. sine – if k is defined, the topography is created by equation
$topo = sin(k * x) + c$.

Parameter x axis, y axis, z axis this parameters define size of the final numpy array in pixels.

Coefficient c defines intersection with y axis.

Parameter r defines radius of simulated sphere. Three-dimensional numpy array with a shape of the the final topography is returned.

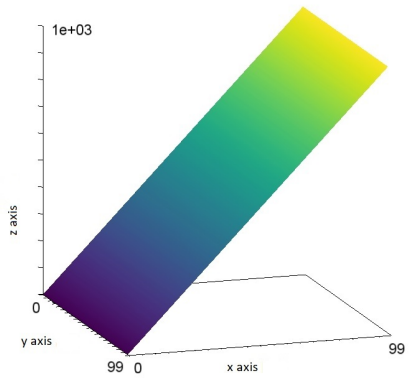

(a) line

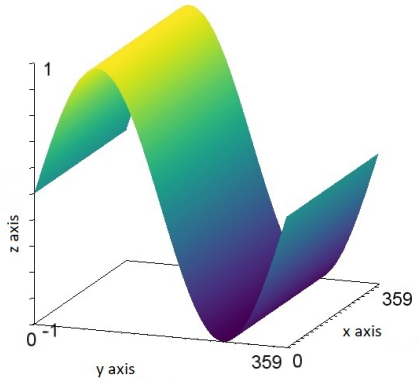

(b) sine

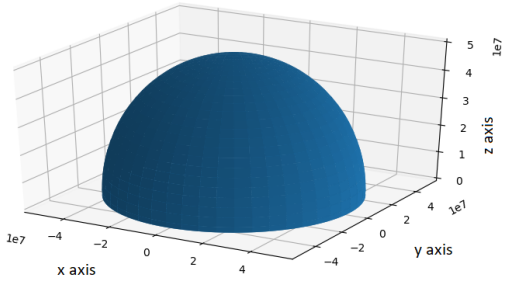

(c) sphere

Figure 3.2: Possible shapes of simulated surface

3.2.2 Create signal

Function create signal generates white-light signal by parameters given to the equation:

$$I(z) = I_B + \gamma I_B exp\left[\left(-\frac{z - z_0}{lc}\right)^2\right] \cos\left[\frac{4\pi}{\lambda_0}(z - z_0) + \varphi_0\right],$$

where I_B is background intensity; is sampling contrast; lc is coherent length of Gaussian spectrum of light source; λ_0 is expected value of wavelength; z_0 is scanning position along z-axis, where envelope of white-light signal is maximum, this value is the topography generated in the previous function; φ_0 is phase difference between reference and object light beam. The parameters of the function are:

Topo here a topography generated in previous function is used.

Fixed step size is parameter where a constant size of scanning step is put. The size is fixed to obtain ideally shaped envelope. Real measurement is influenced by errors caused by noise. The noise is add in next step of this function.

step min, step max are parameters, that define an interval. From this interval is generated random number, which is added to the *fixed step size*. Due to this parameter signal with different scanning position along z-axis is created.

Ib is parameter of background intensity.

Lambda1, lambda2 are starting and ending value of wavelength spectrum.

Phi0 is value of phase difference between reference and object beam.

In next part of the code, the vibrations are suppressed by the approach described in paper [47].

In measuring with white-light sensor, the result contains a large amount of image frames (min. 150/envelope). Between these frames, there should be an equal spatial step but measurement can be influenced by mechanical vibrations. These vibrations can change the step, therefore the signal processing is not as easy as with an equal step size. In this algorithm, a passive compensation of vibrations is used. Therefore, the change of the step size is captured in the measurement of surface topography.

In the first step of the simulation, vibrations are added to the step size. How the signal with an added noise looks is shown in 3.3. The fixed step size is randomly changed, the size of the change is described in 3.2.2. Due to this, the signal with correct order is obtained but sampling interval is changed. However, typical

evaluating algorithms need the uniform sampling step. Hence, the captured signal is interpolated to get the uniform sampling step and increase precision of signal evaluation.

For interpolation we used the the linear interpolation. The equation is described below.

$$I(u) = I_k + \frac{I_{k+1} - I_k}{z_{k+1} - z_k}(u - z_k), \tag{3.9}$$

where u is the desired step between two sequential steps and z_{k+1}, z_k are assigned intensity values. For small amplitudes of vibration, linear interpolation is sufficient to correct signal evaluation unless the vibrations are not too high.

For improving white-light signal, the trigonometrical approximation is used. Every function can be approximated by linear combination of sin and cos [48]. The approximation is described in the following equation:

$$f(z) = a_0 + \sum_{n=N_1}^{N_2} (a_n cos(nz) + b_n(nz)), a, b \in \mathbb{R} \tag{3.10}$$

In application, a dataObject with added vibrations is created, if it is necessary a size of the dataObject is changed. The dataObject can be also created without the added vibration. The linear interpolation is applied to see if the signal improve and than triangular approximation.

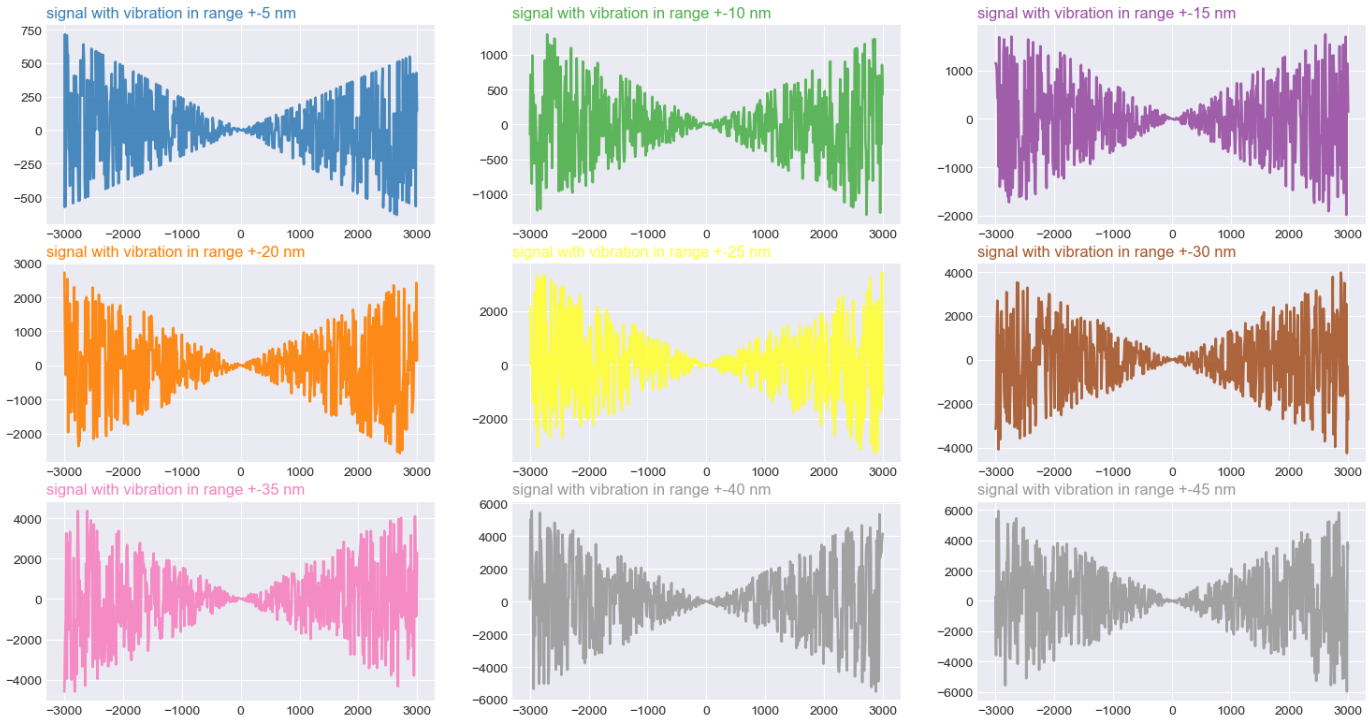

Figure 3.3: Generated signal with added noise in given range. The yellow plot is signal with vibration in range +- 25 nm

3.2.3 Applying white light evaluation

In function "applywli eval" the functions described in 3.1 are applied. The functions are built in ITOM. There is a comparison how the results look for the signal with added vibrations and without them.

At first, the region of interest (ROI) is defined. The region of interest is defined as depth of dataObject. The threshold and axis are set to zero. It is necessary to create empty dataObjects where these dataObjects the data will be saved into.

"reduceData" Reduce data is filter, that extracts a ROI with the relevant data of a WLI envelope. The input dataObject must be 3-dimensional. The output data are copied into dataObject "reduceData". It is necessary to set an envelope axis (done before the assignment). Results are in figure 3.4 and 3.5.

"subtractDC" filter subtracts DC part of the signal from each envelope. The envelopes must be allocated along previously defined axis. Results are shown

in figure 3.6 and 3.7.

"findPeriod" Filter findPeriod helps us to find period of envelopes. Period of the used signal is shown in 3.8.

"multiplyWithSin" This filter multiplies the data stack with complex wave. The output are two dataObjects, one with complex part, the other with real part.

"lowpass" This filter applies low-pass filter on the data. The filter is applied twice to ensure a stable phase.

"calcCOGandPhase" Filter calculates COG and phase (relative to the lock-in wave) of filtered real and imaginary part. This filter has two outputs, one contains the center of gravity of each envelope signal, the other one contains the phase relative to the lock-in wave.

"calcPos" This filter calculates the position of the zero order extremes and returns them.

These filters are applied to the signal with and without added vibrations to evaluate the white-light signals. In the pictures below, the comparison of the signal is shown.

3.2.4 Simulation result

After the function 3.2.3 the comparison of how is the COG and phase changing regarding to the vibration changes.

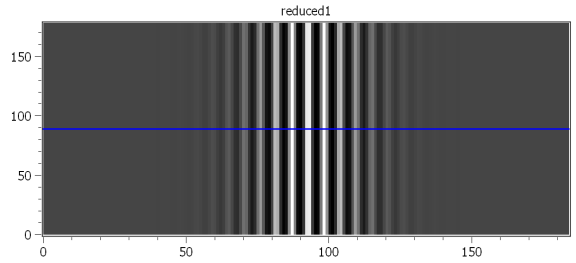

(a) Reduce data - signal without vibration

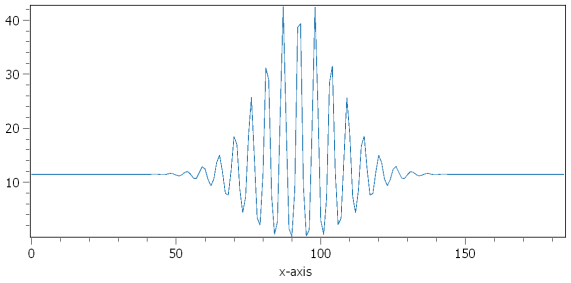

(b) Reduce data - interference envelope after triangular interpolation without vibration

Figure 3.4: Reduced data without vibration

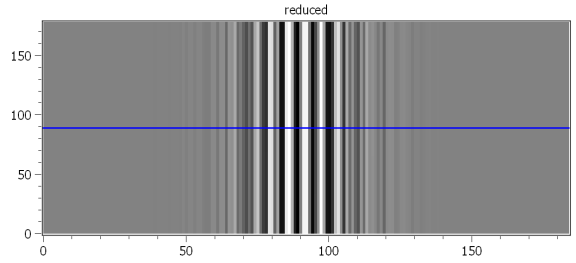

(a) Reduce data - signal with vibration

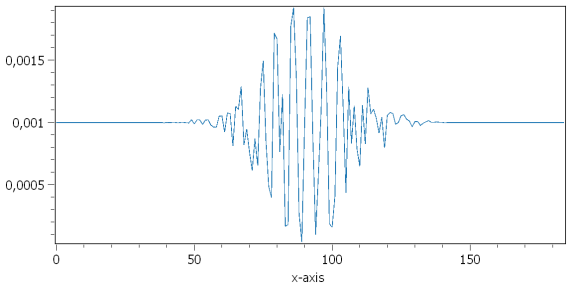

(b) Reduce data - interference envelope after triangular interpolation without vibration

Figure 3.5: Reduced data with vibration

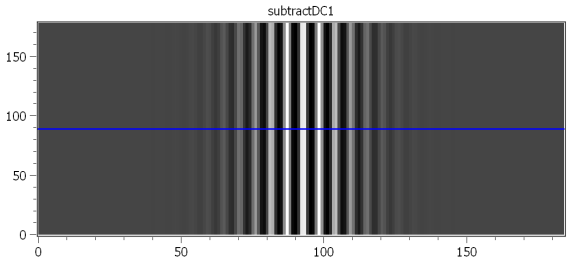

(a) Subtract DC - signal without vibration

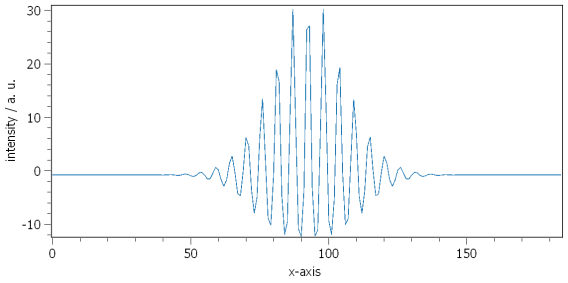

(b) Subtract DC - line cut of three dimensional signal

Figure 3.6: Subtract DC - data without vibration

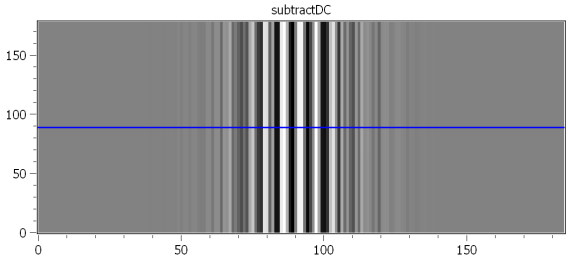

(a) Subtract DC - signal with vibration

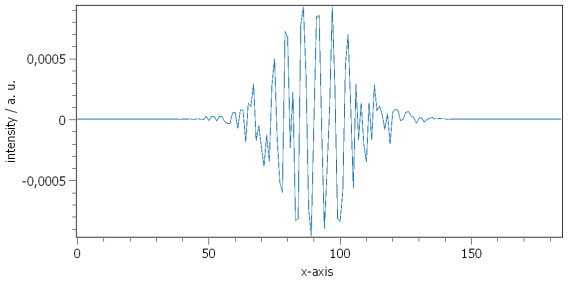

(b) Subtract DC - line cut of three dimensional signal

Figure 3.7: Subtract DC - data with vibration

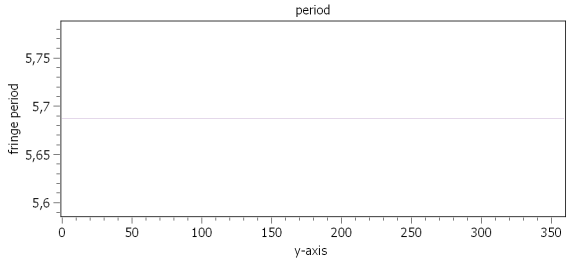

(a) Period of signal without vibration

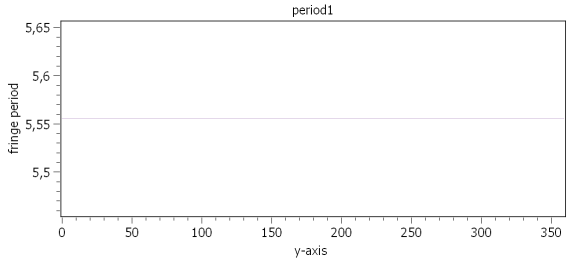

(b) Period of signal with vibration

Figure 3.8: Subtract DC - data without vibration

Period of signal without vibration equals 5.52 s and signal with vibration equals 5.68 s.

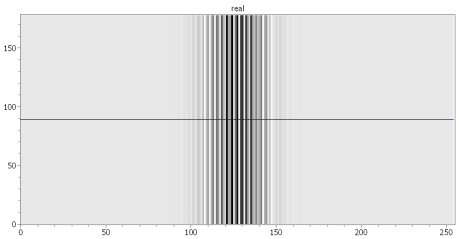

(a) Real part of the signal

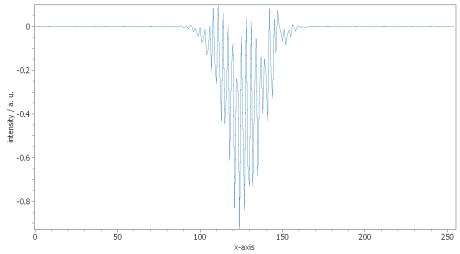

(b) Line cut of the real signal

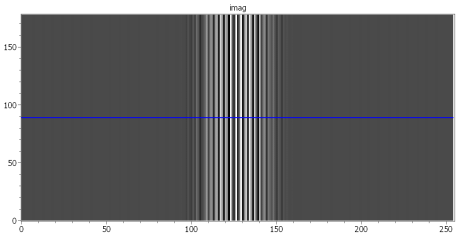

(c) Imaginary part of the signal

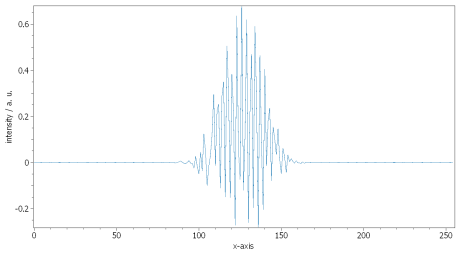

(d) Line cut of the imaginary signal

Figure 3.9: Multiply with sinus - data with vibration

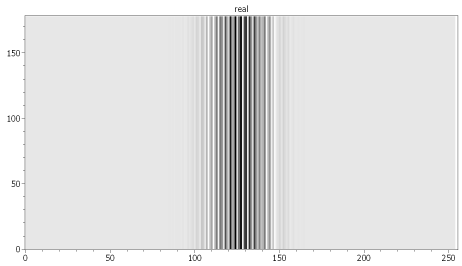

(a) Real part of the signal

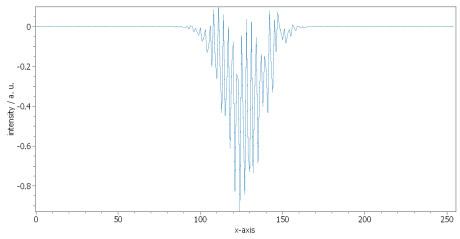

(b) Line cut of the real signal

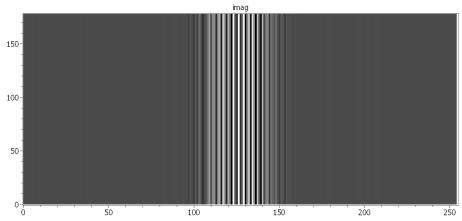

(c) Imaginary part of the signal

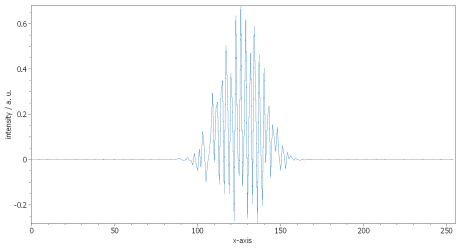

(d) Line cut of the imaginary signal

Figure 3.10: Multiply with sinus - data without vibration

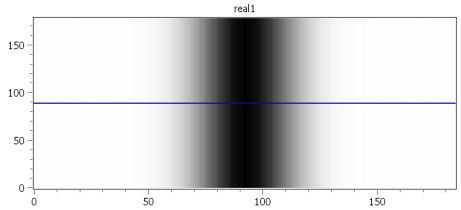

(a) Real part of the signal

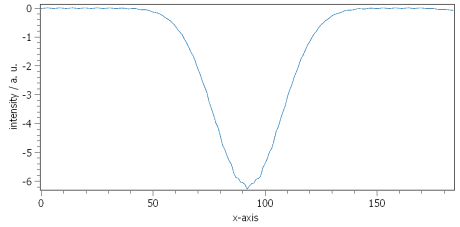

(b) Line cut of the real signal

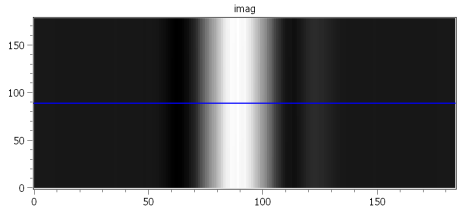

(c) Imaginary part of the signal

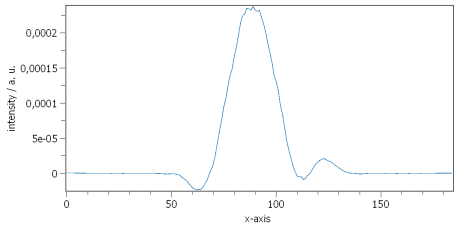

(d) Line cut of the imaginary signal

Figure 3.11: Signal after applying low pass filter - data without vibration

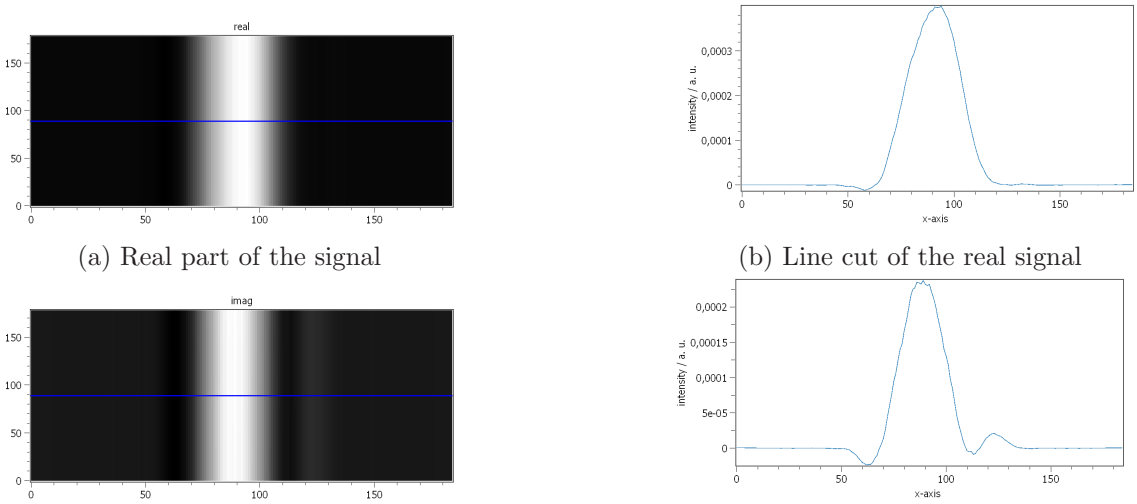

(a) Real part of the signal

(b) Line cut of the real signal

(c) Imaginary part of the signal

(d) Line cut of the imaginary signal

Figure 3.12: Signal after applying low pass filter - data with vibration

The comparison of the signal with and without vibration has significant differences. The difference between center of gravity and zPos is important for evaluation. The difference between zPos and cog should be increasing when there is an increase in the vibration interval, therefore the obtained signal cannot be processed. Same as in measuring, if the measuring setup is shaking, the surface topography is not obtained correctly.

The smaller the difference, the better result should be obtained.

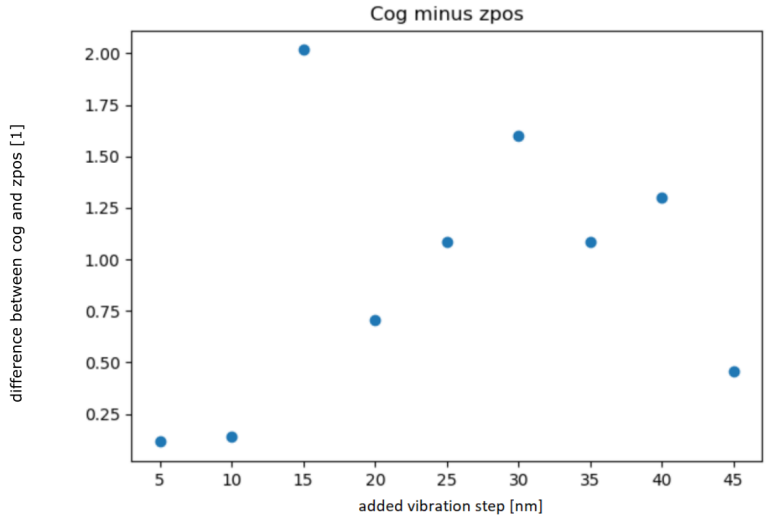

Figure 3.13: Difference in cog - zPos with increasing vibration interval

The difference shown in figure 3.13 is not increasing linearly but only when the vibration interval is small (added step in range plus minus 5 nm and plus minus

10 nm). In other cases, the difference was too big. This simulation was focused on measuring sphere with a diameter 50mm, measured with central wavelength 630 nm. Even though the difference in range more or less 50nm is not very big, the obtained signal has not many similarities with the signal without vibration shown in figure 2.2 as is seen in figure 3.14. The signal has no clear shape and it is impossible to say, where the maximum is. The comparison of the obtained results lead to confirmation that it is necessary to have nanopositioning device to obtain results with high precision, because higher step disparities lead to incorrect results.

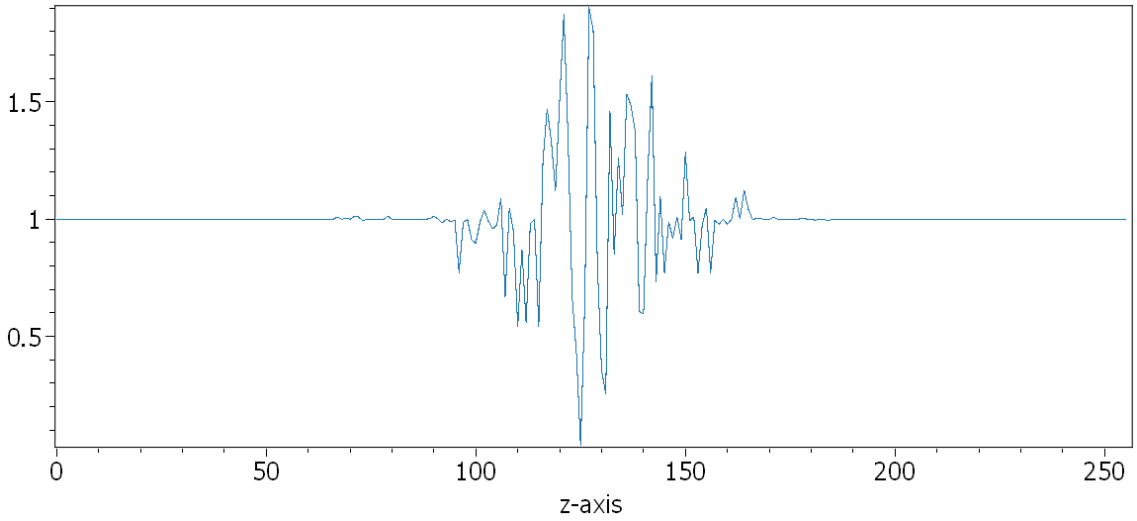

Figure 3.14: Signal with added vibration in range -50 to 50 nm

4 The verification on NPMM-200

4.1 Description of measuring device

NPMM-200 is shortcut for Nanopositioning and Nanomeasuring Machine. NPMM-200 is situated in Institute of Applied Optics, University of Stuttgart. Originally, it was built at the University of Illmenau. This device is able to measure samples with volume 200 mm * 200 mm * 25 mm. The machine has glass-ceramical metrological frame. To the frame, an interferometrically controled stage for high precision measurement and sensor holder are attached. The sensor can be changed regarding to the measuring requirements.

4.2 Sensors

To keep a subnanometer resolution, there is a necessity to use proper sensors. The NPMM has an advantage - the user can change the sensor. The original sensors were built at the Technische Universität Illmenau, where the NPMM-200 comes from. All the sensors originally created for Nanomeasuring Machines are described in paper [49]. Only those we have worked with are described in this thesis.

4.2.1 Fixed-focus sensor

The sensor used in Nanomess is based on a laser hologram unit, but in contrary to an autofocus sensor with fixed objective lens. The original creators of this sensor were able to achieve a high tenacity as well as a good thermal and mechanical stability of the probe. Therefore, they were able to get subnanometrical resolution.

The sensor has two lenses; the transmitting one and the receiving one. Both are focused to a focus point. Around the point, there is a sensing window. If the subject is not in the window, the sensor cannot detect it.

This particular sensor was combined with camera microscope and CCD sensor, therefore the view to the laser spot and the area around is obtained in real time.

The creators of the sensor were able to manage high repeatability of the sensor as well as high precision in standard measuring step from 7 nm to 700 nm. Because of the microscope lens, it is necessary to be careful about the steepness of the sample. If the steepness is to high, there is a possibility of collision between the microscope lens and the sample. Hence, the working distance of the lens needs to be known. In the original setup, the creators used a lens with a short working distance. In our setup, a lens with a long working distance is used (lens 50X Nikon CFI60 TU Plan Epi ELWD with 11.0mm working distance).

4.2.2 White-light sensor

White-light sensor is based on the white-light interferometry. White-light sensor allows us to capture data in parallel. With this measuring, a vast collection of data (approximately 2 million points) is obtained, which may cause trouble with signal processing. Another complication while measuring with white-light sensor is a limitation in a measuring range. If the measuring range is bigger than $100\mu m$, there might be problems with finding zero optical path difference (ZOPD).

A measuring area (field of view) is 800 x 800 μm^2, 2048x2048 pixels. The working distance is dependent on the lens used.

4.3 Working principle

In paper [50] and [51] the working principle is described. To the thermally stable metrological frame made of Zerodur®. The working principle is is that the frame with sensor is stable, whereas the sample is moving on a three-axis stage beneath the frame with the sample. The sample is located on a top part called the mirror corner. The movement is driven by direct electronic voice coil drives.

With the interferometers, the position and the angular deviation of the mirror corner in view of the metrological frame is measured. While constructing the interferometer, it is necessary to avoid Abbe errors. Abbe errors are caused when angular errors in the motion systems combine with the offset between the point of interest and the source of the errors. Abbe errors amplify small angular errors, errors magnify with the distance from origin of the error. [52].

For high-precision measuring, it is necessary to minimize Abbe errors. The NPMM is minimizing errors in three-dimensional space by controlling the angular deviation of the mirror corner over the whole measuring range. The main interferometer axis intersects at the Abbe-Point. If the measured sample is small enough,

the sample can be placed inside the mirror corner, thereby eliminating all Abbe offsets. With National-Instruments PXI FPGA-Modules, the position and the angular deviations are controlled.

The signals from interferometers are corrected with the data from calibrated sensors monitoring conditions of the environment (temperature, pressure and humidity) inside the measuring chamber. It is also necessary to monitor the refractive index of the air for high accuracy. For that reason, the measuring machine is situated inside a vacuum chamber. The chamber is standing on vibration damping feet. Vacuum reduces the influence of refractive index modulation on the interferometric measurement.

The NPMM is controlled by a measuring program in ITOM. The sensors used for testing the machine 4.2. The signal from the sensor is combined with measured position along z-axis. This approach helps us to avoid linearity errors.

Overall parameters of the machine:

Positioning volume	200 mm x 200 mm x 25 mm
Interferometer resolution	0.02 nm
Sample size	max 310 mm x 310 mm x 90 mm

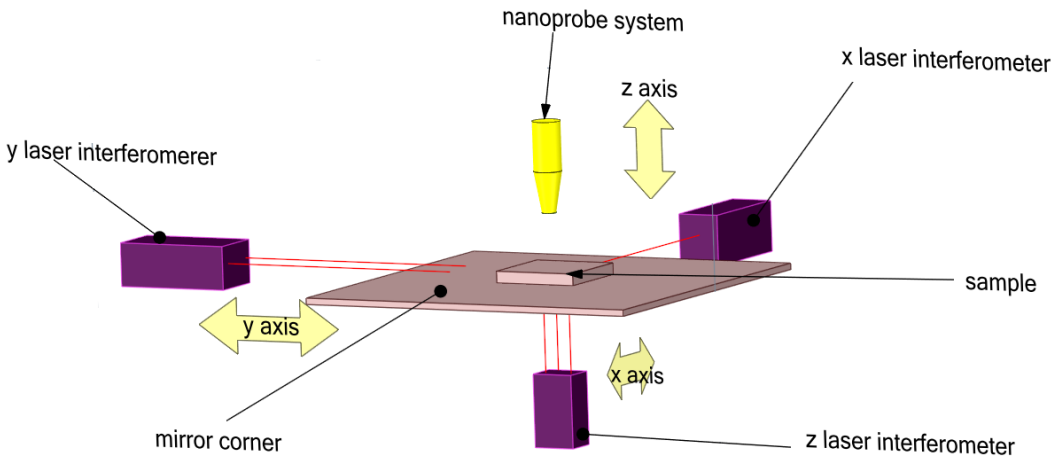

Figure 4.1: 5 Interferometers monitoring the position and angles of the corner mirror.

4.4 Measuring approaches

There are two measuring approaches - line scan and circle scan. At first, the four points on the sample border are found, then the function *circle fit* is applied. Circle fit finds the function that "best" fits the points (least square method for circle). The function returns center and radius [53].

Line scan scans the surface of the sample by moving along parallel lines with a regular spacing over the entire surface of the sample. Before the measurement starts, it is necessary to find the center of the sample. Before running the measurement, it is determined with how many lines the surface is scanned and the angle of how the lines are oriented. An example of measurement is shown in figure 4.2.

Circle scan scans the surface of the sample by moving in concentric circles with a regular spacing over the entire surface of the sample. Circle scan is suited for scanning spherical samples with a small inclination and for measurement of flat samples.

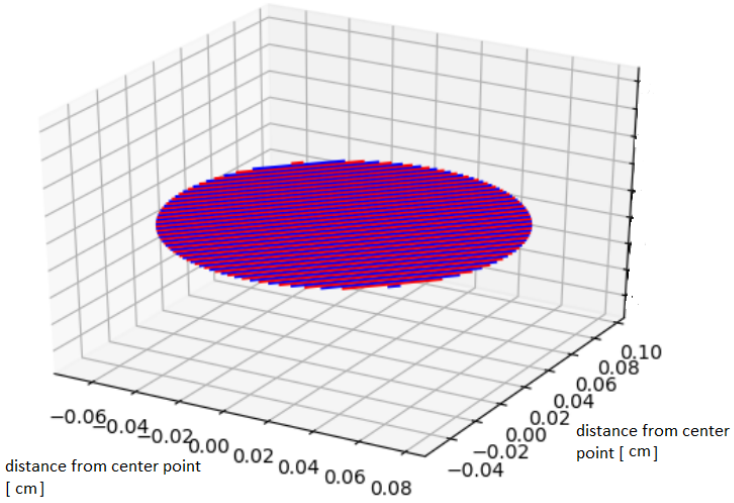

Figure 4.2: Visualisation of "line scan", number of lines 60, orientation 45°

When the measuring was running, there was one "forbidden point" and it was necessary to avoid this point. If the scanning position got to this point, the whole measurement failed. It was probably caused by certain defects on the mirror.

4.5 Data processing

Data measured with ITOM software are processed in the MATLAB software. There is a code for evaluating NPMM200 data measured in ITOM. It was necessary to modify the code for every measurement with different shape.

In the first step, the measured points are depicted. If the tested shape is a sphere, the fit function SphereFit is used on the measured data to create the "best" fit sphere. In following step, the Delaunay triangulation is used to generate triangular mesh with the shape of the sample. Next, the three dimensional plot with the trimesh function is created. This plot views the whole sphere. The z values of the best fit sphere are subtracted from the measured z values. The subtracted z value corresponds with the value of z axis from the sphere generated from SphereFit. With these steps, the real surface of the measured sphere is obtained. In the measurement dataset, there is an item "sum signal", which is proportional to the reflected intensity captured by the focus sensor. If the sum signal is included as the fourth parameter, the result is a three dimensional plot with surface defects of the sample.

With this sample, two measurement were running, second measurement was rotated by 120 °. Final results needed to be compared with each other. The comparison is made by averaging the rotated measurements, creating an interpolation of the scattered data, and then displaying.

If the measured sample is flat, it is crucial to find how is the sample tilted. The tilt is caused by an imperfect mounting. Again, the interpolation of scattered data is made and data are displayed. Evaluation of the freeforms and aspherical surfaces is based on the same principle as evaluating the flats.

4.6 Measurement with fixed - focus sensor

For the testing, multiple samples made of different materials were used. The easiest shape to measure - a sphere - was measured twice. One sphere made of glass, needles to say the specification of the glass and coating was not known; the second glass was made of Zerodur®. The Zerodur®sphere has worse reflectivity than a standard glass. Therefore, the measurement was more complicated. The measuring was also done on an asphere. The asphere had no specification about itself, therefore, it was not easy to find the proper settings. The last measured shape was a flat. The flat was polished with a peak-to-valley value 50 nm. The complication to measuring this sphere was a proper mounting into the measured device.

4.6.1 Sphere with radius 43.401 mm

The first measured sample was a spherical mirror with radius 43.401 mm. Because of its size and material, the measurement of the whole surface was not possible, because the sensor was able to capture the reflected signal without problems.

The evaluated signal showed that the surface of the mirror is very scratched. Measuring on a very scratched surface can cause problems with reflection - the reflected signal is not strong enough to be recorded by the sensor. Therefore it is necessary to control the velocity of the motion and measure with low velocity. Results are shown in figures 4.3, 4.4, 4.5.

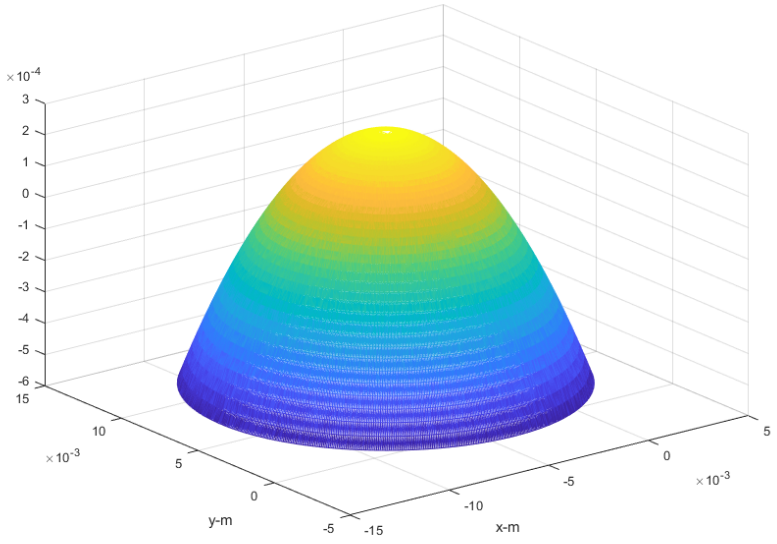

Figure 4.3: Surface of the sample only from measured data

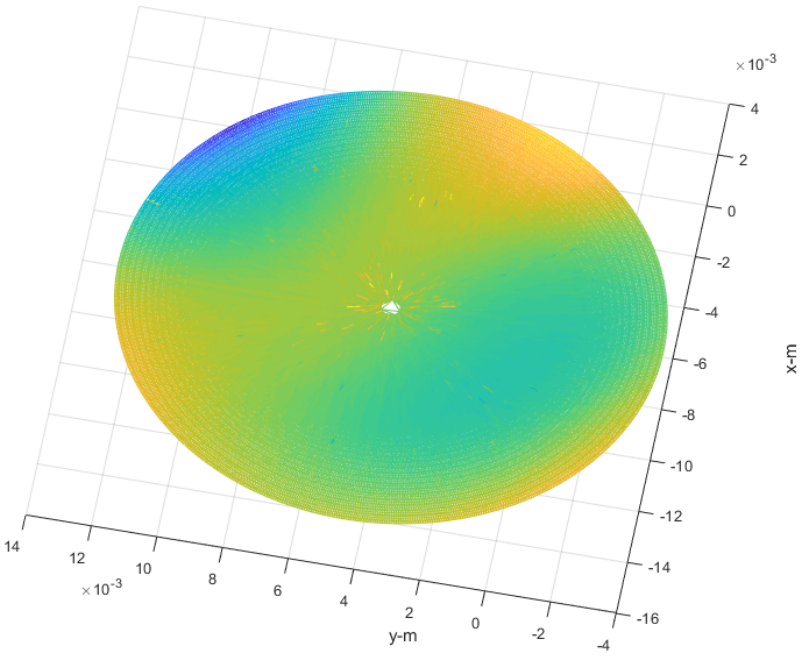

Figure 4.4: Surface of the sample after subtracting ideal sphere from measured surface

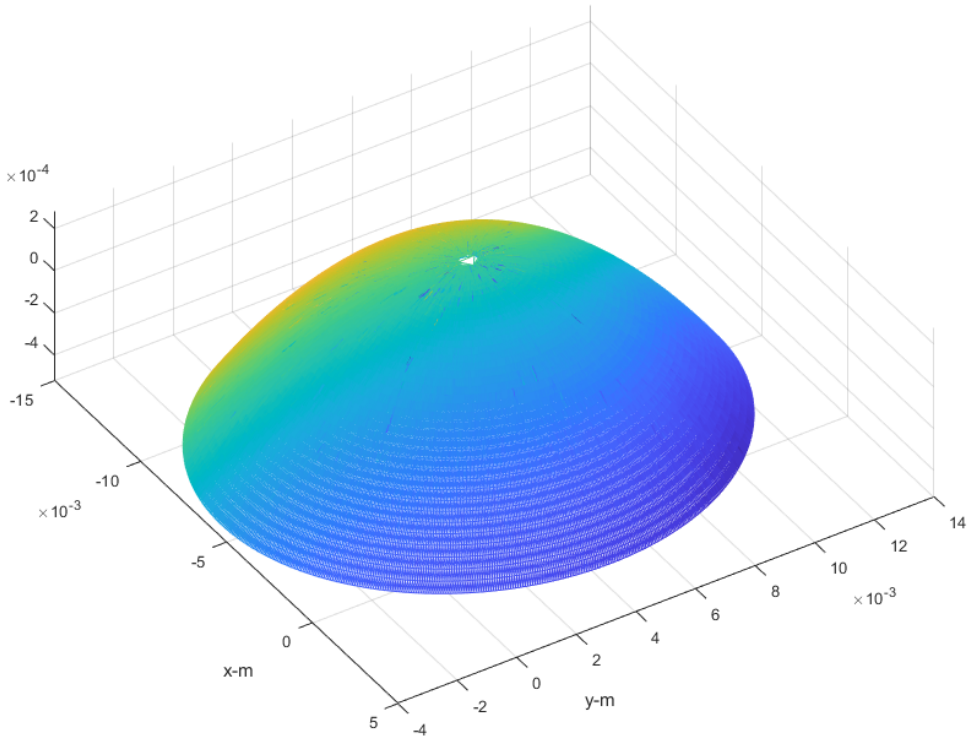

Figure 4.5: Sum signal, in this view are the scratches most visible

4.6.2 Sphere made of Zerodur®with radius 100mm

The sphere made of Zerodur®is used as a reference sphere in interferometers. The Problem with this sample was a low reflectance. Even though the signal was amplified, it was impossible to measure the whole sample surface because the fixed focus sensor was not able to record the laser light.

In this measurement, three measurements (figures 4.6) rotated by 120°were run. All three measurements were evaluated with the similar algorithm that is described in paper [54]. Three measurements are averaged, the data obtained in the previous step are evaluated as if it was a standard sphere measurement.

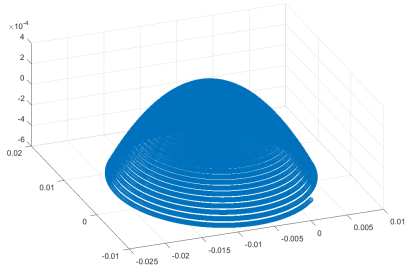

(a) Zerodur®sphere rotated by 110°

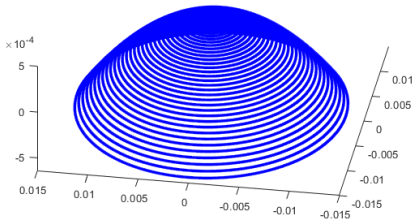

(b) Zerodur®sphere rotated by 230°

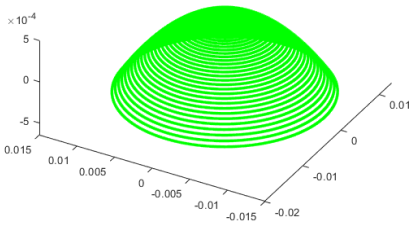

(c) Zerodur®sphere rotated by 350°

Figure 4.6: Measurement of Zerodur®sphere with different rotation

The sphere calculated from all surfaces is shown in figure 4.7.

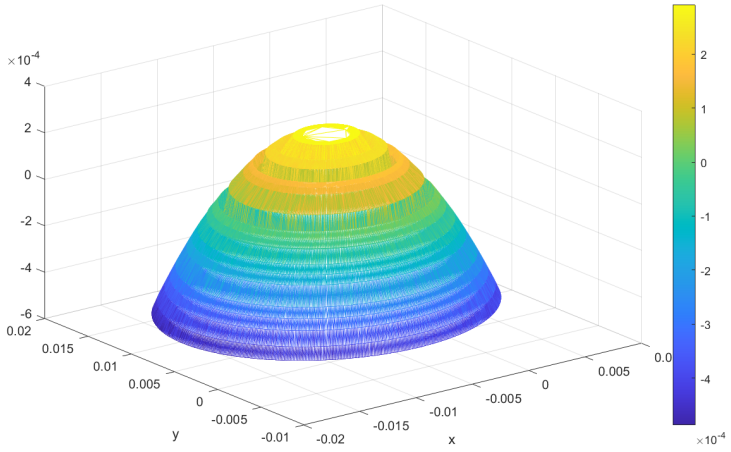

Figure 4.7: Zerodur®sphere after evaluation

In 4.7 is obvious, that in the area close to the y-axis is a peak. The peak is in similar places in every measurement, even though the sphere is rotated. That made us think there is a problem with the measuring device.

The error could originate from the steepness of the surface.

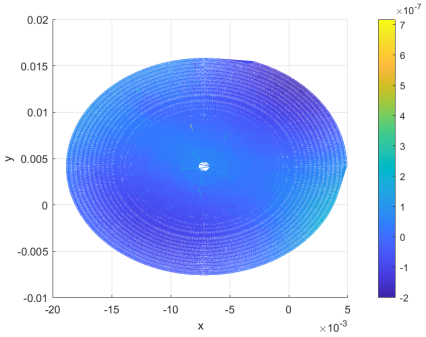

(a) Sum signal rotated by 110°

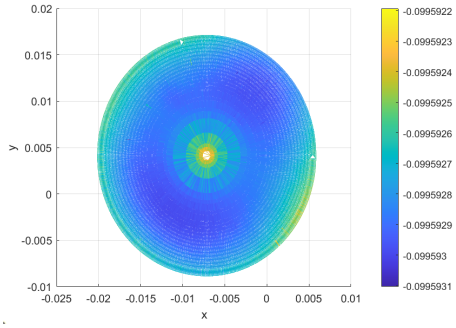

(b) Sum signal rotated by 230°

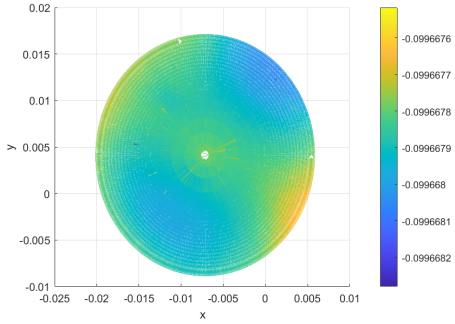

(c) Sum signal rotated by 350°

Figure 4.8: Sum signal from taken from different rotation

4.6.3 Asphere "Schmidt plate"

An asphere "Schmidt plate" is a 40 years old asphere. There is no documentation of this sample, therefore, this sample was measured with NPMM-200 as well as with a commercial measuring device ZYGO.

The measurement was run in two modes - line scan (4.9 and circle scan. The radius of the sample was measured with a caliper. The radius equals to 45 mm, although the measurement with NPMM-200 was limited to 38 mm, as the borders were scratched too much for the fixed focus sensor to receive the reflected signal.

The shape of the asphere is well readable with line scan 4.9. With circle scan, the measurement of the shape is devalued because of the missing lines.

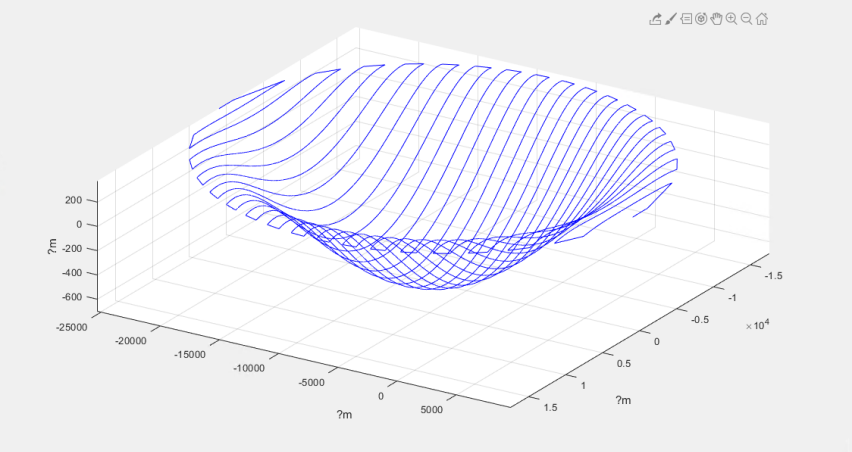

Figure 4.9: Topography measured with "line scan"

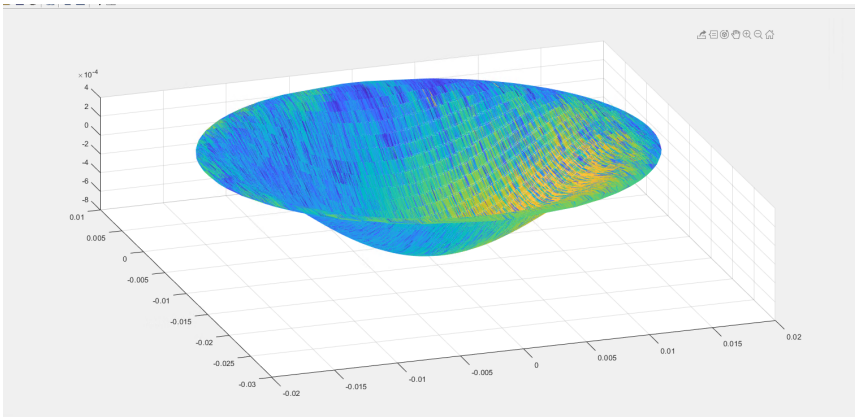

Figure 4.10: The surface sample measured with "line scan"

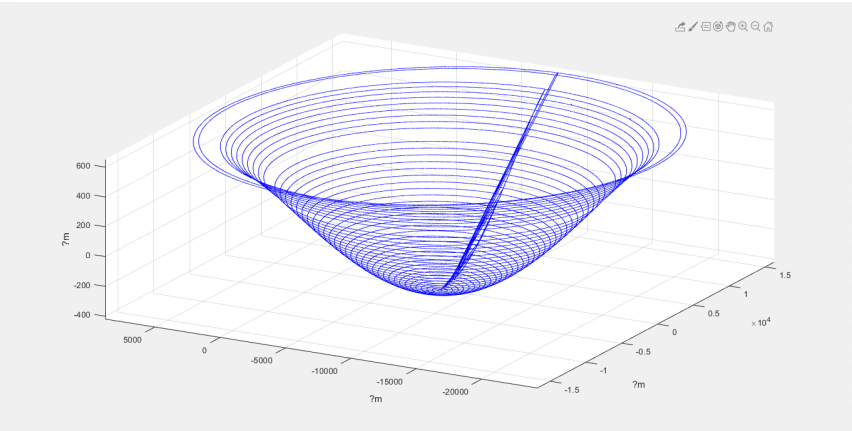

Figure 4.11: Topography measured with "circle scan", the line is caused by moving of the sensor

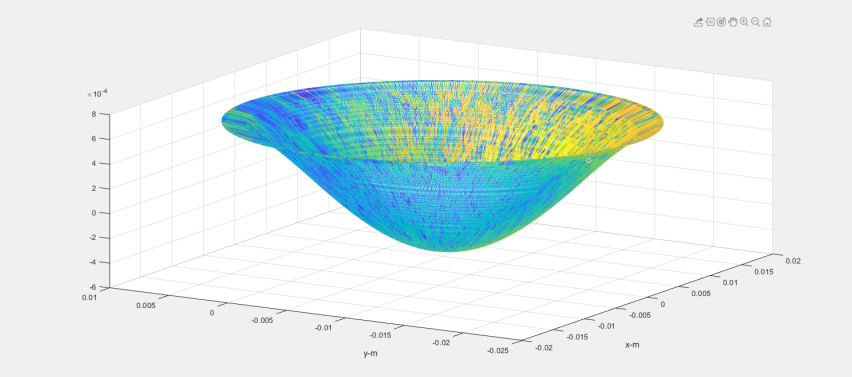

Figure 4.12: The surface sample measured with "circle scan"

The peak-to-valley value in measurement with line scan was 4e-7 m. The same peak-to valley value was obtained in circle-scan measurement. The only encountered problem during the measurement was that the reflected signal was not strong enough.

For proving if the results are correct, the sample was measured using a commercial measuring device - ZYGO. With ZYGO, only surface topography can be inspected, not the shape. Results are shown in figure 4.13. Peak-to-valley value in THE center was approximately 87 nm, around the edge it was approximately 681 nm and in the inflection point, it was approximately 552 nm.

4.6.4 Measuring flat with polished surface

Measuring the flat was quite complicated due to uneasy manipulation and mounting. Dimension of the sample:

surface highest evenness	10 nm PV
diameter	150 mm
Thickness	30 mm

The sample was mounted using a kinetic mount. Mounting is shown in figure 4.14. The kinetic mounting can be used as a very accurate mounting device. One rigid body is placed onto another one. The second body does not add any constraints to the original body as well as not does not cause any instability. It is possible, with an exact number of contact points, allow the degrees of freedom as necessary.

The standard rigid body has six degrees of freedom (DOF). With every added mounting point, the DOF is reduced [55] [56]

This exact mount has three building blocks. All of the blocks contain a differently situated glass balls. The first one is a ball on surface, the second one is a ball in

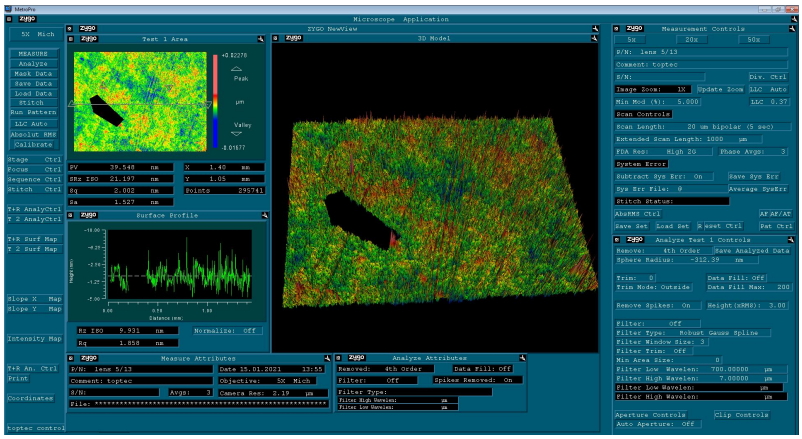

(a) Topography in the center

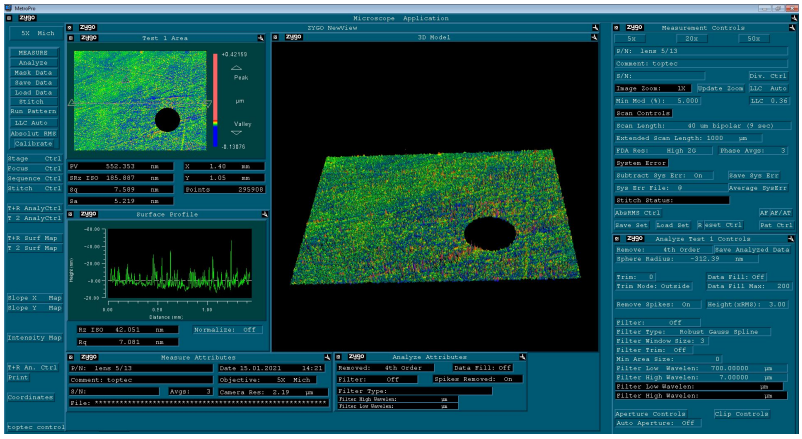

(b) Topography in the inflection point

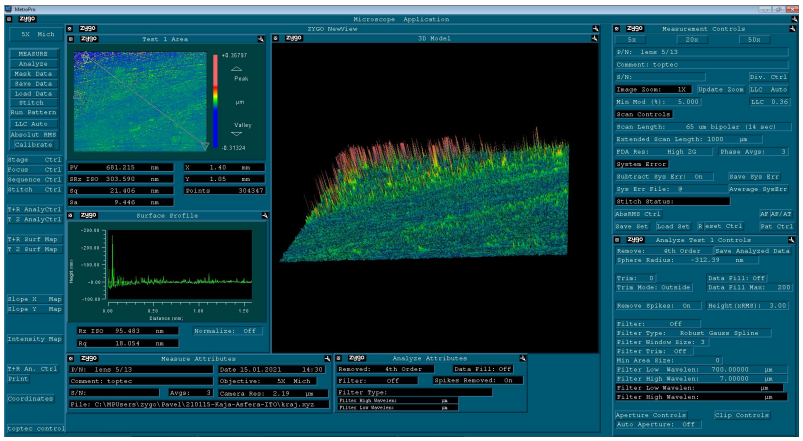

(c) Edge part of the asphere - not measured with NPMM-200

Figure 4.13: Topography measured with ZYGO

vee, and the third one is a ball in trihedral socket. The setup has three degrees of freedom; it is has great stability and resolution.

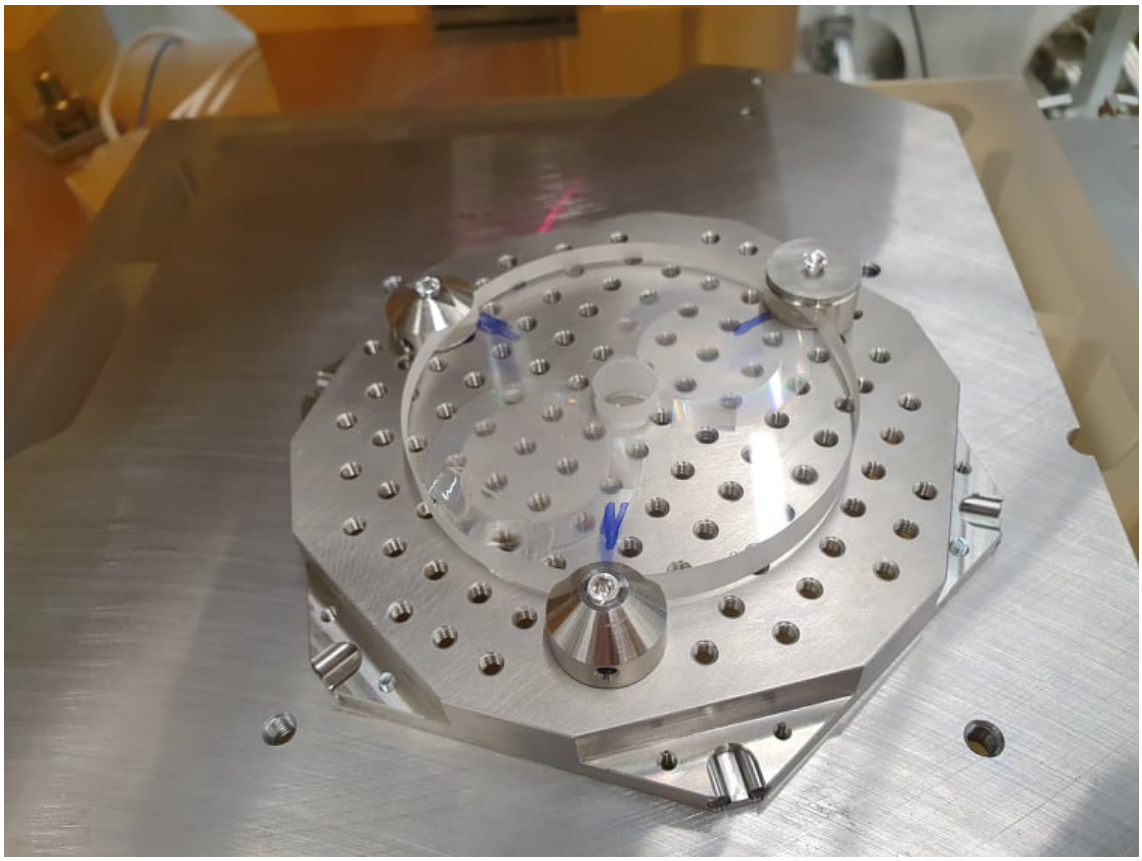

Figure 4.14: Kinetic mount

Multiple circle and line scan measurements were run to get the best possible results. The first set of results is shown in figure 4.15. The comparison between the NPMM-200 and ZYGO white- light interferometer is shown in 4.16

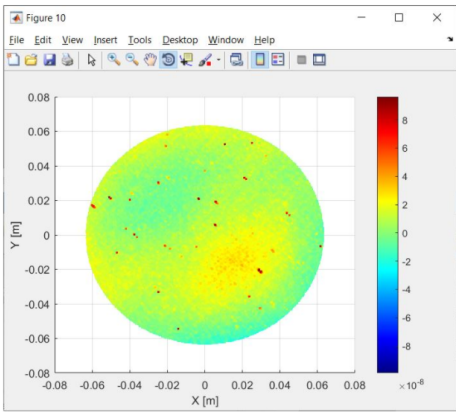

(a) Sample measured with line scan

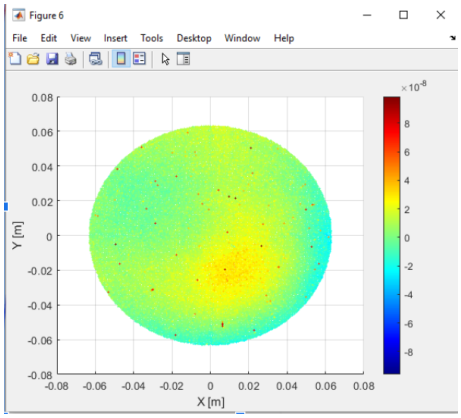

(b) Rotated sample measured with circle scan

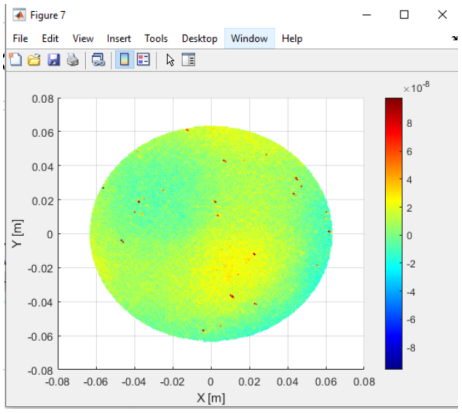

(c) Sample measured with line scan, rotated holders

Figure 4.15: Surface topography of the sample

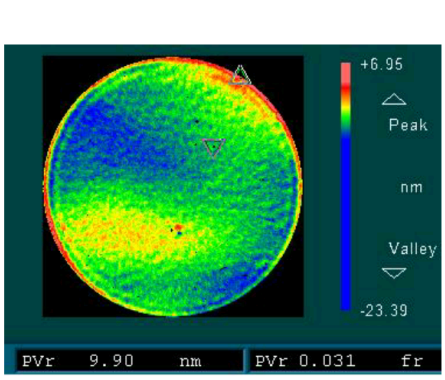

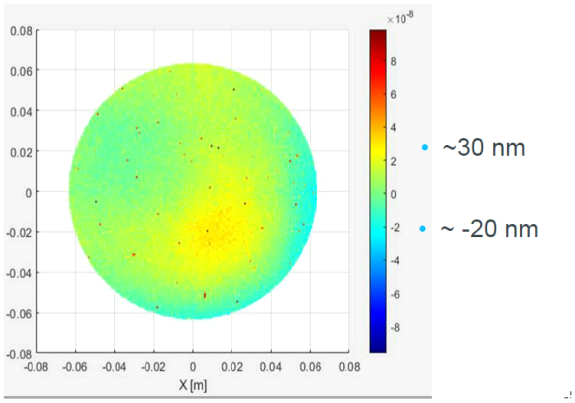

Figure 4.16: The comparison between ZYGO WLI and NPMM - 200

The red dots are in different positions but there are red and turquoise area, that are not changing their location even when the sample 's position has changed.

That is caused by an error in the measuring device. Multiple changes were made in the setup - modifying the mounting to make it more stable, applying calibration function, stitching multiple measurements. All these steps led to conclusion that the error in measurements was caused by the measuring device.

4.7 Measuring with white-light sensor

For testing the white-light sensor, the NPMM - 200 is in setup similar to Mirau interferometer. The illumination source is a white-light diode. The working principle of the sensor is described in 4.2.2. The results are calculated in ITOM with the algorithm described in 3.1.

The measurement was made with 50 nm step for 25 measurements in each step. With the 25 figures, the influence of the vibrations is reduced by averaging them.

4.7.1 Results

The sample measured with WLI sensor was USAF 1951. USAF is a standard tool for inspecting resolution. It is a plane with drawn groups of lines. These lines are drawn horizontally and vertically. The groups are numbered; the bigger the number is, the better the resolution. As long as the lines are not blurred and they can be counted, the group can be declared as resolved.

As noticeable in figure 4.17a, the last revolvable group is with number 7. In a closer look to zPos of the real measurement 4.18b, it is seen that the group 7-6 well resolved. That means that the resolution is 2.2 um.[57]

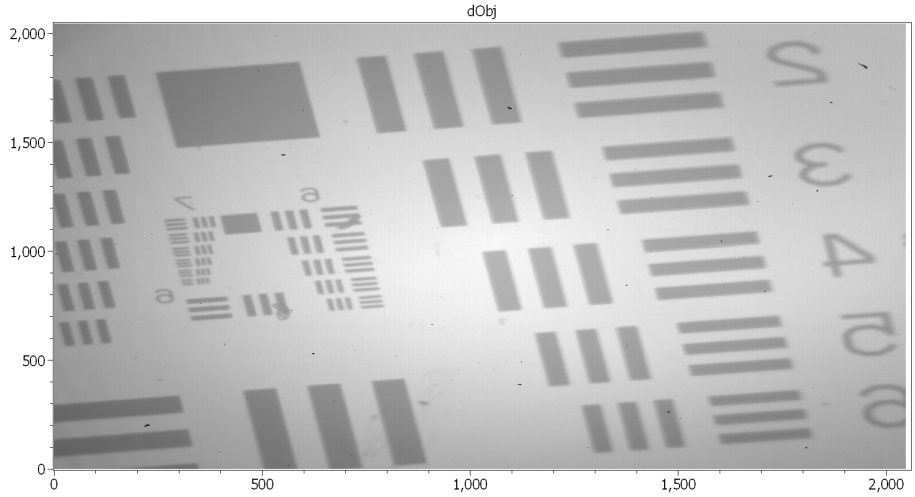

(a) Result of measurement with WLI sensor

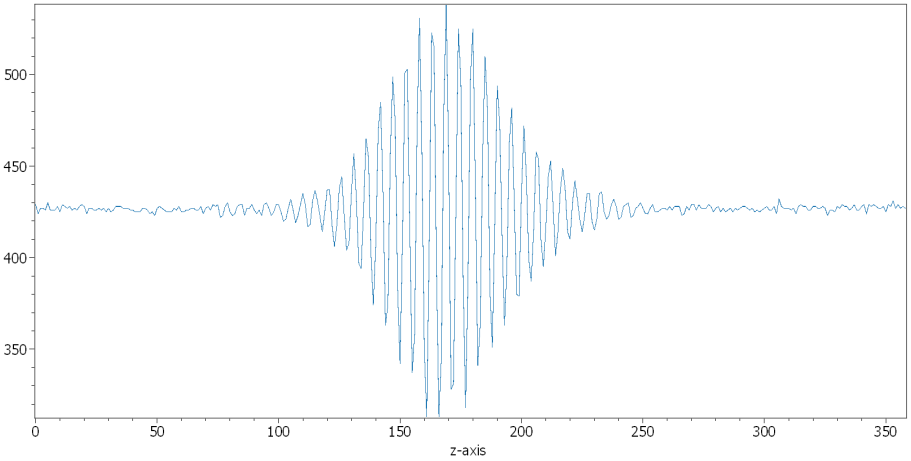

(b) Obtained signal of the image

Figure 4.17: Measurement of USAF 1951 with WLI and obtained signal

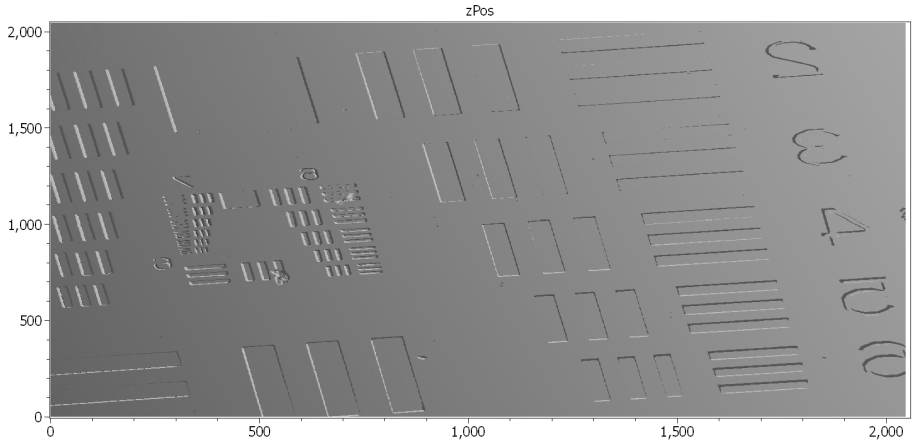

(a) zPos from WLI measurement

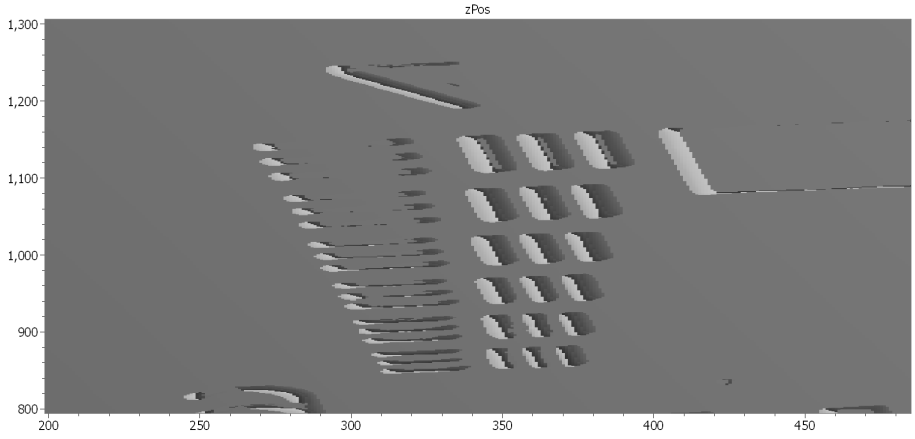

(b) Zoomed zPos in WLI measurement

Figure 4.18: zPos from WLI measurement

4.8 Overall evaluation of the device

With the focus sensor fixed, the device is able to measure smaller samples with precision over 1 um. During the first testing, there were problems with measuring of samples of larger diameter. Most likely, the cause of the problems was the defect at the controlling mirrors. Another problem was encountered while mounting a heavy sample. The weight made the device tilt. A Fixed-focus sensor is also not suitable for samples with a low reflectvity.

The NPMM-200 has two measuring approaches - line scan and circle scan. The circle scan is better to use with spherical samples. The advantage of the line scan is you can use it with any shape. In both approaches, it is necessary to find a center of the sample; in circle scan, the centre is the starting position. If the center is not found properly, the measurement is tilted. In both approaches, it is needed to avoid

a point (x = -18,98 a y = -5,51) where the measurement fails without a reason, but it has already been included into the code. Now the you are informed, that the measurement goes through this point and the line or circle including it will be avoided.

Measurement with white-light sensor is more prone to vibration than measurement with fixed-focus sensor. The fixed-focus sensor measures as long as the signal is found. For suppressing the influence of vibrations in the white-light sensor approach, the measurement is done multiple times and the signal is averaged. Currently, the resolution with white-light sensor is over 3um, but with proper tuning the resolution is supposed to be over a one micrometer.

Conclusion

The outcomes of the thesis were: become acquainted with principles of measuring surface topography; create a numeric tool for analysing coherent scanning interferometry; test, analyse and optimize a profilometer NPMM-200 and evaluate the obtained results.

The first task of the thesis was to get to know contactless methods used to measure surface topography. The first chapter informs on the basics of illumination and light properties. There is information about basic light sources used in measuring surface topography, the properties of the light - such as coherence, diffraction and interference. These findings are used in the methods described in chapter two.

The Second chapter deals with measuring methods based on interference. There are facts about the Michaelson, Mach - Zender, Newton, Fizeau and Mirau interferometer setups. These interferometrical setups are described as all of them can be used in measuring surface topography and most of them can be used to build a whit -light interferometer. White-light interferometry is not similar to the standard interferometers because in this approach, the light with low coherence is used. Unlike with standard interferometry, where the single fringes are evaulated, in the white-light inteferometry, the wavelet of the signal is evaluated. The roughness on the surface and vibration on the measuring device are negatively influencing the wavelet evaluation.

How the vibrations influence the signal from the white-light interferometer is described in Chapter three. Especially for this detection, a numerical tool was developed. The tool takes a surface by user's choice. The user chooses the shape and size of the sample. The sample can be flat, sphere or sine shape. From the given shape, the signal is generated. It is necessary to add other parameters into the function generating signal, which is needed to create white-light signal - background intensity, sampling contrast, coherent length of the source of the light, central wavelength and phase difference between object and reference beam. The function takes one more output - the vibration range. The vibration range gives us the maximum

range of the vibration of the measuring device. The function creates a signal, adds vibrations to the signal and then applies algorithms that reduce the vibrations. In the next part of the code, the dataset with reduced vibrations is taken as an input. The algorithms calculate a maximum of the signal and center of gravity of the signal and subtract these two values. The smaller the difference, the better the evaluation with vibrations. In the shown example, a sphere with 50 mm radius was evaluated. With the central wavelength 630 nm and coherence length 0.01mm, the maximum vibration amplitude range allowing to obtain good results was += 10 nm. These results prove it is necessary to have a nanopositionning measuring machine to obtain precise results of the shape of the sample.

The last chapter presents the development of a profilometer NPMM-200. The profilometer is able to change the position of the measured sample in range of nm. This device is also special in its construction, as it is made of thermally stable materials. For preserving the stable refraction index, it is closed in the vacuum chamber. It also has replaceable sensors. The measurements were done with a fixed-focus sensor and a white-light sensor. With the fixed-focus sensor, it was necessary to find a proper approach to measure different shapes of the samples. For measuring a sphere, it was a better option to use circle scan (the sample is not moving, the probe is scanning in concentric circles), because the moving step is well definable and the following evaluation is less complex. For the samples like aspheres, freeforms or flats, the results obtained with line scan are better. In the linescan, the user determines with how many and how oriented lines is the surface going to be scanned. With linescan, we can measure critical parts more precisely. Using the fixed-focus sensor, it was found out that there was an error in the measuring device. This error was caused by tilting of the sample holding a part of the device. This error led to sending the device to the original creators to Technical University of Illmenau, where the error was solved. The measurement with the white-light sensor is still in development nowadays. An issue of this modification is the vibrations. As revealed by the simulating tool, the vibrations with bigger amplitude than 10 nm can ruin the measurement. The vibrations are intended to be compensated with the device mounting. The vibrations occurring in device can be caused by resonance of the device. For avoiding these errors, the sample is measured multiple times (at least 25 times) and the influence of the vibrations is suppressed. If this approach is not sufficient, the triangular interpolation is used. For now, the best axial resolution of the device with white-light sensor was 2.2 um. The improvements are still ongoing because the current axial resolution is far behind the expected values.

Bibliography

[1] VILLANUEVA, John Carl. Radiation from the Sun [online]. March 19, 2010 [cit. 2021-04-05]. Available from: https://www.universetoday.com/60065/radiation-from-the-sun/

[2] Visible light. NASA SCIENCE [online]. [cit. 2021-02-05]. Available from: https://science.nasa.gov/ems/09visiblelight

[3] PALERMO, Elizabeth. Who invented a ligh bulb? Live Science [online]. Aug 17, 2017 [cit. 2021-03-31]. Available from: https://www.livescience.com/43424-who-invented-the-light-bulb.html

[4] ARECCHI, Angelo V., Tahar MESSADI a R, John KOSHEL, 2007. *Field guide to illumination*. Bellingham: SPIE PRESS BOOK. ISBN 9780819467683.

[5] MAGONCIA, JB. How does an LED work? *CircuitBread* [online]. September 19, 2019 [cit. 2021-04-07]. Available from: https://www.circuitbread.com/tutorials/how-does-an-led-work

[6] JAIN, Deepnika. Principles of LED. *Toppr* [online]. November 5, 2017 [cit. 2021-04-07]. Available from: https://www.toppr.com/bytes/principles-of-led/

[7] Light Emitting Diode What are LEDs and How Do They Work? *ROHM semiconductors* [online]. [cit. 2021-04-07]. Available from: https://www.rohm.com/electronics-basics/leds/what-are-leds

[8] ELECTRICAL4U. White Light Emitting Diode or White LED Light. *Electrical 4 U* [online]. October 27, 2020 [cit. 2021-04-07]. Available from: https://www.electrical4u.com/white-led/

[9] MALÝ, Petr, 2008. *Optika*. V Praze: Karolinum. ISBN 978-80-246-1342-0.

[10] SALEH, Bahaa E. A. a Malvin Carl TEICH, 1996. *Základy fotoniky: Fundamentals of photonics*. Praha: Matfyzpress. ISBN 80-85863-00-6.

[11] PASCHOTTA, Rüdiger, 2008. *Field Guide to Lasers*. Bellingham: SPIE PRESS BOOK. ISBN 9780819478269.

[12] Active Medium. *Fraunhofer Institute for Laser Technology ILT* [online]. [cit. 2021-04-09]. Available from: https://www.ilt.fraunhofer.de/en/studies/laser-tutorial/active-medium.html

[13] PASCHOTTA, Rüdiger. Neodymium-doped Gain Media. *RP Photonics Encyclopedia* [online]. [cit. 2021-04-09]. Available from: https://www.rp-photonics.com/neodymiumdopedgainmedia.html

[14] List of laser types, 2001-. In: *Wikipedia: the free encyclopedia* [online]. San Francisco (CA): Wikimedia Foundation [cit. 2021-04-09]. Available from: https://en.wikipedia.org/wiki/Listoflasertypes

[15] OSTROVSKY, Andrey S., 2006. Coherent-Mode Representation of Optical Fields and Sources. *Coherent-Mode Representations in Optics*. SPIE Press, s. 1-14. ISBN 9780819463500.

[16] *The mutual coherence function* [online], 2004. Italy [cit. 2021-03-21]. Available from: http://www.arcetri.astro.it/ mosca/radioastronomy/corso/node43.html

[17] ELLIS, Jonathan D., 2014. *Field Guide to Displacement Measuring Interferometry*. FG30. SPIE PRESS BOOK. ISBN 9780819497994.

[18] TKACZYK, Tomasz S. *Field guide to microscopy*. Bellingham, Washington 98227-0010 USA: SPIE, 2010.

[19] PASCHOTTA, Dr. Rüdiger. *RP Photonics Encyclopedia: Coherence Time* [online]. [cit. 2021-03-25]. Available from: https://www.rp-photonics.com/coherencetime.html

[20] ABRAMOWITZ, Mortimer. *Diffraction of Light* [online]. [cit. 2021-04-15]. Available from: https://www.olympus-lifescience.com/en/microscope-resource/primer/lightandcolor/diffraction/

[21] *Učební text k přednášce UFY102 - Difrakce světla* [online]. Fyzikální ústav, MFF [cit. 2021-04-15]. Available from: http://fu.mff.cuni.cz/biomolecules/media/files/courses/Difrakce.pdf

[22] HECHT, Eugene a William T. RHODES. *Optics*. 4th ed. San Francisco: Pearson/Addison Wesley, 2002. ISBN 0-8053-8566-5.

[23] URONE, PP. Limits of Resolution: The Rayleigh Criterion [online]. 2012 [cit. 2021-04-15]. Available from: https://opentextbc.ca/openstaxcollegephysics/chapter/limits-of-resolution-the-rayleigh-criterion/

[24] BORN, Max a Emil WOLF. *Principles of optics: electromagnetic theory of propagation, interference and diffraction of light*. 7th (exp.) ed. Cambridge: Cambridge University Press, 1999. ISBN 0-521-64222-1.

[25] ISO Surface Roughness. *Engineerings Edge* [online]. [cit. 2021-5-14]. Available from: https://www.engineersedge.com/manufacturing/$_{i}so_{s}urface_{r}oughness_{s}ymbols_{t}erminol$ 04 − 19].$Availablefrom$: $https$: $//www.proinex.cz/cs/blog/10mereni -$ $drsnosti - povrchu$

[26] STOUT, Ken a Liam BLUNT. *Three Dimensional Surface Topography*. Huddersfield: Elsevier Science, 2000. ISBN 978-1-85718-026-8.

[27] LEACH, Richard, 2011. *Optical Measurement of Surface Topography*. Berlin Heidelberg: Springer-Verlag. ISBN 978-3-642-12012-1.

[28] Štoll I., *Elektřina a magnetismus*, Vydavatelství ČVUT, Praha 2003

[29] The Michelson Interferometer. BC Campus [online]. [cit. 2021-04-19]. Available from: https://opentextbc.ca/universityphysicsv3openstax/chapter/the-michelson-interferometer/

[30] MALACARA, Daniel, 2007. *Optical shop testing*. Third edition. New York: John Wiley Sons. ISBN 978-0-471-48404-2.

[31] ZETIE, K. P., S. F. ADAMS a R. M. TOCKNELL, 2000. *How does a Mach-Zehnder interferometer work? Physics Education*. 35(1), 46–48. Available from: doi:10.1088/0031-9120/35/1/308

[32] LÉDL, V., P. PSOTA, P. VOJTÍŠEK a R. DOLEČEK, 2015. Digitální holografická interferometrie. Liberec: Technická univerzita v Liberci. ISBN 978-80-906324-0-0.

[33] HARIHARAN, Parameswaran, 2003. *Optical interferometry*. 2nd ed. Amsterdam: Academic Press. ISBN 01-231-1630-9.

[34] *Guideline for Use of Fizeau Interferometer in Optical Testing* [online]. 1999-02-01 [cit. 2021-04-21]. Available from: https://llis.nasa.gov/lesson/717

[35] WYANT, James C. *White Light Interferometry*. Optical Sciences Center, University ofArizona, Tucson, AZ 85721.

[36] PAVLÍČEK, Pavel, 2011. Measurement uncertainty of White-light interferometry on optically rough surfaces. AWREJCEWEC, Jan. *Numerical Simulations of Physical and Engineering Processes*. s. 491-502. ISBN 978-953-307-620-1.

[37] PAVLÍČEK, Pavel a Ondřej HÝBL, 2008. White-light interferometry on rough surfaces— measurement uncertainty caused by surface roughness. *Applied Optics*. **47**(16), 2941-2949. Available from: doi:https://doi.org/10.1364/AO.47.002941

[38] JOVIĆ, O., OMANOVIĆ, D., ZELIĆ, M., PIŽETA, I. (2015). Center of Gravity (COG) Method as a Tool in Processing of Voltammetric Signals. *Electroanalysis*, **27**(10), 2347–2356. doi:10.1002/elan.201500065

[39] *CENTER OF MASS* [online]. Free Books, Physical Audio Signal Processing [cit. 2021-04-23]. Available from: https://www.dsprelated.com/freebooks/pasp/CenterMass.html,

[40] VORBURGER, T.V., Methods for Characterizing Surface Topography. 2010. MOORE, Duncan T., *Tutorials in Optics* pg. 137 - 151.

[41] THWAITE, E.G, *Surface Topography Measurement and Analysing*, 1982, *Applied physics*, Royal Melbourne Institute of Technology. Available from: https://www.sciencedirect.com/topics/physics-and-astronomy/electron-microscopes

[42] MARION, JERRY B. Electrons and photons, Physics in the Modern World, Second Edition, 1981 [cit. 2021-04-20].

[43] Antonio Abate, et. al.,*Nanomaterials for Solar Cell Applications*, Elsevier,2019,ISBN 9780128133378, https://doi.org/10.1016/B978-0-12-813337-8.00024-2.

[44] ISMAIL, Ahmad Fauzi , Wan Norharyati Wan SALLEH, Norhaniza YUSOF,*Synthetic Polymeric Membranes for Advanced Water Treatment, Gas Separation, and Energy Sustainability*,Elsevier, 2020,ISBN 9780128184851, https://doi.org/10.1016/B978-0-12-818485-1.09987-1.

[45] ITOM software - itom [online], 2000. Stuttgart: Institut für Technische Optik [cit. 2021-03-28]. Available from: https://itom.bitbucket.io/

[46] HAHN, Robin a ET AL, 2017. *Single-shot low coherence pointwise measuring interferometer with potential for in-line inspection.* Stuttgart, Germany, 2017. DOI:10.1088/1361-6501/aa52f1.

[47] TERESCHENKO, Stanislav, Peter LEHMANN, and Lisa ZELLMER, 2016. Passive vibration compensation in scanning white-light interferometry. Applied Optics. Institute for Materials Engineering, University of Kassel, Moenchebergstrasse 3, 34109 Kassel, Germany.

[48] VRBIK, Jan. Trigonometric Approximation (Fourier series). Spartan.ac.brocku.ca [online]. Brock University [cit. 2020-10-22]; http://spartan.ac.brocku.ca/ jvrbik/MATH3P60/fourier.pdf

[49] MANSKE, E. et al. *New applications of the nanopositioning and nanomeasuring machine by using advanced tactile and non-tactile probes.* Measurement Science and Technology. (Volume 18, Number 2); https://doi.org/10.1088/0957-0233/18/2/S27.

[50] SCHOBER, Christian, Christof PRUSS, Alois HERKOMMER, and Wolfgang OSTEN. *The NPMM-200: large area high resolution for freeform surface measurement*, Proc. SPIE 11478, Seventh European Seminar on Precision Optics Manufacturing, 1147807 (8 July 2020); https://doi.org/10.1117/12.2564918.

[51] BALZER, Felix Gerhard, 2015. *Entwicklung und Untersuchungen zur 3-D-Nanopositioniertechnik in großen Bewegungsbereichen.* Illmenau. Dissertation work. Technische Universität Ilmenau.

[52] COLLINS, Danielle, February 6, 2019. What is Abbé error and how does it affect linear systems? Linear motion tips [online]. [cit. 2021-02-20]. Available from: https://www.linearmotiontips.com/what-is-abbe-error-and-how-does-it-affect-linear-systems/

[53] RANDY, Bullock. Least-Squares Circle Fit [online]. In: . University Corporation for Atmospheric Research, 2017-02-17 [cit. 2021-02-22]. Available from: https://www.dtcenter.org/sites/default/files/community-code/met/docs/write-ups/circlefit.pdf

[54] SEITZ, Günther, 2005. *Absolute interferometric measurement of non rotational symmetric surface erros.* Carl Zeiss SMT AG: DGaO Proceedings.

[55] CAMPBELL, Rob. *The Principle of Kinematic Constraint*. Practical Precision [online]. 2016-02-21, [cit. 2021-03-01]. Available from: https://practicalprecision.com/kinematic-constraint/

[56] HORVATH, Nicolas W., Matthew A. DAVIES a Steven R. PATTERSON, 2019. Kinematic mirror mount design for ultra-precision manufacturing, metrology, and system level integration for high performance visible spectrum imaging systems. *Precision Engineering*. (60), 535-543. ISSN 0141-6359,. Available from: doi:doi.org/10.1016/j.precisioneng.2019.09.011

[57] How to read an USAF1951 target? *OptoWiki* [online]. [cit. 2021-04-12]. Available from: https://www.optowiki.info/faq/how-to-read-an-usaf1951-target/